16

EMC Aspect as Important Parameter of New Technologies

Irena Kováčová and Dobroslav Kováč
Technical University of Košice
Slovak Republic

1. Introduction

Equipment disturbances and errors have become more serious as a consequence of the growth of the electronic circuit complexity. According to new technical legislation and also economic consequences, the electromagnetic compatibility (EMC) concept of all products must be strictly observed (Montrose & Nakauchi, 2004). It must start with the specification of the equipment performance and end with the equipment installation procedures. The importance of the electromagnetic compatibility (EMC) of all electrical products has grown rapidly during the last decade. The environment is increasingly polluted with electromagnetic energy. The interference output into the surroundings is doubled every three years, and covers a large frequency range.

2. EMC couplings

The EMC concept is defined as competence of functional coexistence of electrical and also biological devices or systems at the same time and in such a way that even though they are located in the common electromagnetic environs, there is no relevant influencing factor of their normal functionality (Vaculíková & Vaculík, 1998). Devices can but don't need to have the mutual dependence. On the one hand the systems must be robust against the other systems influences, but on the other hand they must not affect adversely the normal functionality of other devices (Fig. 1). On one side, interferences are deliberately or involuntarily produced. The place of their origin is called interference source. On the other side, devices can be hindered in their function by such interferences. Those objects are called interference objects.

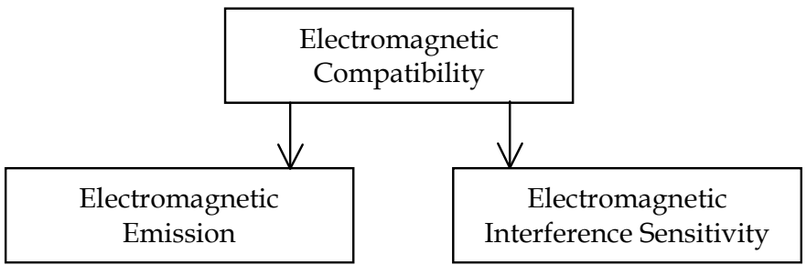

Fig. 1. Division of EMC into key aspects

Each system utilized in practice is exposed to disturbing effects generated by the various sources such as, for example, power switches, contactor tapes, relays, arc furnaces, high frequency heating, commutator motors, and power semiconductor converters, etc, see Fig. 2.

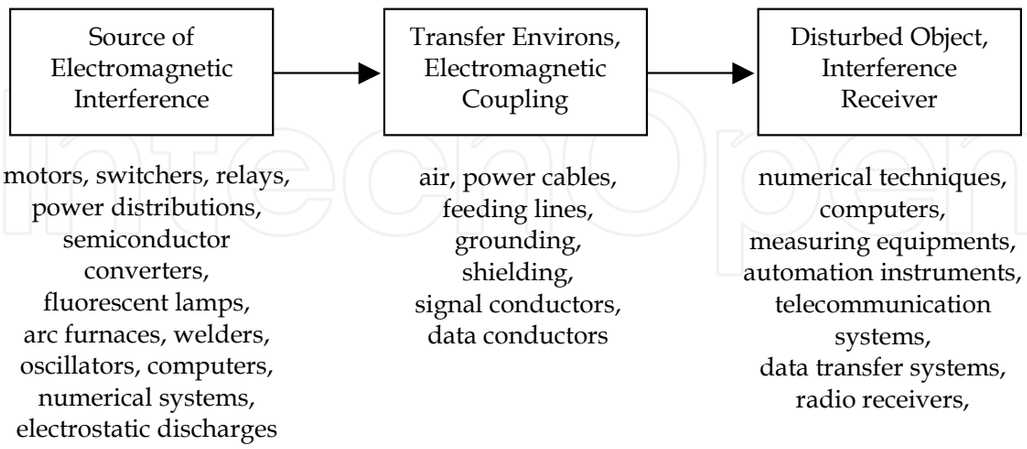

Fig. 2. Basic chain of EMC and examples of individual section types

Noise surrounding influences, which are manifested by unfavorable linkages, interference noises, resonant and transient states, can cause not only incorrect equipment functionality, but also its destruction in extreme cases. The interference source can be for instance a power semiconductor converter or motor. Interference is produced in the interference source getting into electronics in undesirable ways and is due to various effects distorting signals. Transmission can be direct, for example by galvanic coupling between interference source and interference sink. Interference can be spread through air or via ducts, or coupled inductively or capacitively into signal lines. Mutual electromagnetic coupling of individual electrical equipments can be realized by several ways as shown in Fig. 3.

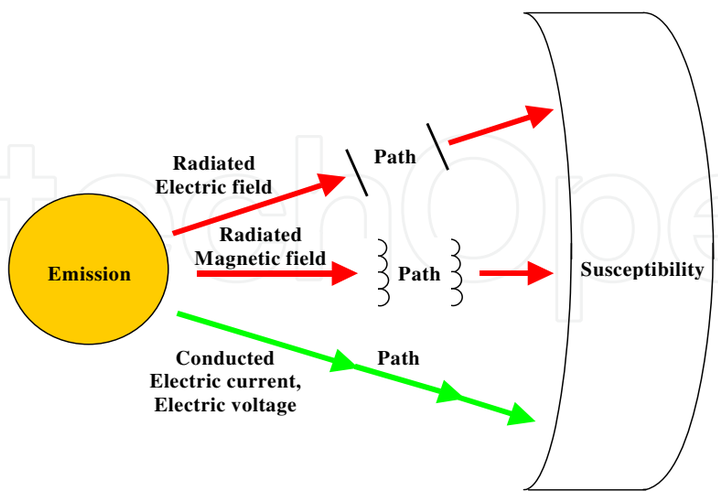

Fig. 3. Ways of mutual electromagnetic coupling

From the viewpoint of the theoretical analysis it is evident that the radiated energy transfer between individual investigated equipments is done by the following ways: inductive coupling, capacitive coupling, galvanic coupling, electromagnetic coupling.

3. Inductive coupling

Inductive coupling is typical for two and more galvanically separated electric loops at the moment when the smaller one is driven by a time variable current creating the corresponding time-variable magnetic field (Kůs, 2002). In such case their mutual intercircuit effect is expressed as a function of the slope of the current increase or decrease, circuit environmental magnetic property as well as circuit geometric dimensions.
To predict the intercircuit inductive coupling, our focus will be on two electric loops l_1 and l_2 with currents i_1 and i_2. We will try to determine the effect of loop l_1 on loop l_2 (Fig. 4).

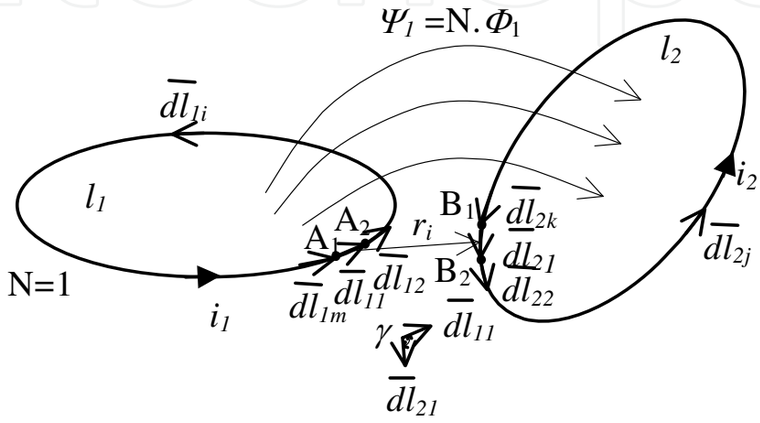

Fig. 4. Investigated loops

According to the Maxwell's equation for a quasi-stationary magnetic field

$$rot\ \overline{E} = -\frac{\partial \overline{B}}{\partial t} \quad \text{and following its integral form} \quad \int_S rot\ \overline{E}.d\overline{S} = -\int_S \frac{\partial \overline{B}}{\partial t}.d\overline{S} = -\frac{\partial}{\partial t}\int_S \overline{B}.d\overline{S} \tag{1}$$

and after applying the Stoke's theorem, we obtain the equation for the induced voltage

$$u_{i2} = -\mathbf{N}.\frac{\partial \phi_1}{\partial t} = -\frac{\partial \psi_1}{\partial t} = -M\frac{\partial i_1}{\partial t} \tag{2}$$

where M is the coefficient of the mutual inductance. For the magnetic flux Φ_1 the equation

$$\phi_1 = \oint_{l_2} \overline{A}_2.d\overline{l}_2 \tag{3}$$

is valid, where $\overline{A}_2$ is the vector of the magnetic field potential created by the current i_1. We can calculate the value of this vector by the following equation:

$$\overline{A}_2 = \frac{\mu.i_1}{4\pi}\oint_{l_1}\frac{d\overline{l}_1}{r_{12}}\,. \tag{4}$$

After substituting the last equation with the equation valid for the magnetic flux ϕ_1 and then for induced voltage u_{i2}, the next relations are obtained:

$$\phi_1 = \oint_{l_2}\left[\frac{\mu.i_1}{4\pi}\oint_{l_1}\frac{d\bar{l}_1}{r_{12}}\right].d\bar{l}_2 = \frac{\mu.i_1}{4\pi}\oint_{l_1}\oint_{l_2}\frac{d\bar{l}_1.d\bar{l}_2}{r_{12}} \tag{5}$$

$$u_{i2} = -\frac{\partial\left(\frac{\mu.i_1}{4\pi}\oint_{l_1}\oint_{l_2}\frac{d\bar{l}_1.d\bar{l}_2}{r_{12}}\right)}{\partial t} = -\frac{\left(\frac{\mu}{4\pi}\oint_{l_1}\oint_{l_2}\frac{d\bar{l}_1.d\bar{l}_2}{r_{12}}\right)\partial i_1}{\partial t} = -M\frac{\partial i_1}{\partial t}\ . \tag{6}$$

For the practical use, it is more advantageous to express the induced voltage in the form of a differentials:

$$u_i = -\frac{di}{dt}.\sum_{\mathrm{i}=1}^{m}\sum_{j=1}^{k}\frac{\mu}{4\pi}\frac{dl_{1i}.dl_{2j}.\cos\gamma_{dlij}}{r_{ij}} \tag{7}$$

If we know the geometrical dimensions of the investigated loops (Fig. 5) and want to determine their mutual inductive coupling then we can use the next equation (8) for the induced voltage. It is based on the 3D Cartesian coordinate system.

$$u_i = -\frac{di}{dt}\sum_{\mathrm{i}=1}^{m}\sum_{j=1}^{k}\frac{\mu}{4\pi}\frac{(\mathbf{A}_{x2i}-\mathbf{A}_{x1i}).(\mathbf{B}_{x2j}-\mathbf{B}_{x1j})+(\mathbf{A}_{y2i}-\mathbf{A}_{y1i}).(\mathbf{B}_{y2j}-\mathbf{B}_{y1j})+(\mathbf{A}_{z2i}-\mathbf{A}_{z1i}).(\mathbf{B}_{z2j}-\mathbf{B}_{z1j})}{\sqrt{\left(\left(\mathbf{B}_{x1j}+\frac{|\mathbf{B}_{x2j}-\mathbf{B}_{x1j}|}{2}\right)-\left(\mathbf{A}_{x1i}+\frac{|\mathbf{A}_{x2i}-\mathbf{A}_{x1i}|}{2}\right)\right)^2+\left(\left(\mathbf{B}_{y1j}+\frac{|\mathbf{B}_{y2j}-\mathbf{B}_{y1j}|}{2}\right)-\left(\mathbf{A}_{y1i}+\frac{|\mathbf{A}_{y2i}-\mathbf{A}_{y1i}|}{2}\right)\right)^2+\left(\left(\mathbf{B}_{z1j}+\frac{|\mathbf{B}_{z2j}-\mathbf{B}_{z1j}|}{2}\right)-\left(\mathbf{A}_{z1i}+\frac{|\mathbf{A}_{z2i}-\mathbf{A}_{z1i}|}{2}\right)\right)^2}} \tag{8}$$

For a global solution of the inductive coupling part of the EMC problem, inside the overall electric power system, it is necessary to analyze the circuit globally focusing on mutual intercircuit inductance coupling. The result is the following integral-differential system of equations:

$$\begin{aligned} u_{cc1} &= R_{c1}.i_1 + L_{c1}.\frac{di_1}{dt} + \frac{1}{C_{c1}}\int i_1.dt + \sum_{\substack{j=1\\ j\neq 1}}^{k} u_{ij} \\ &\vdots \\ u_{cck} &= R_{ck}.i_k + L_{ck}.\frac{di_k}{dt} + \frac{1}{C_{ck}}\int i_k.dt + \sum_{\substack{j=1\\ j\neq k}}^{k} u_{ij} \end{aligned} \tag{9}$$

For this purpose it is very suitable to explore the existing simulation programs such as for example the PSPICE program utilized worldwide.

In the next part, we will try to determine the effect of the one-quadrant impulse converter on the sensing circuit as shown Fig. 5. The circuit dimensions are a = 0.2 m, b = 0.3 m, c = 0.1 m, d = 0.05 m, e = 0.005m. The radius of the copper wires is R = 0.0006 m and the relative permitivity of the circuit environment is μ_r = 0.991. Electrical parameters of the simulation circuit are R_Z = 11.66 Ω, L_Z = 400 μH, R = 10 Ω, R_G = 100 Ω and U_{CC} = 70V. The IGBT transistor Q was switched on at the frequency 10 kHz and the switch on/off ratio was 0.5.

The inductance of the first and second loops are given as

$$L_1 = L_{e1} + L_{i1} = \frac{\mu_0 b}{\pi}\ln\frac{a-R}{R} + \frac{\mu_0 a}{\pi}\ln\frac{b-R}{R} + \frac{\mu.2.(a+b)}{8\pi} = 1.294\ \mu H \tag{10}$$

$$L_2 = L_{e2} + L_{i2} = \frac{\mu_0 c}{\pi}\ln\frac{d-R}{R} + \frac{\mu_0 d}{\pi}\ln\frac{c-R}{R} + \frac{\mu.2.(c+d)}{8\pi} = 0.294\ \mu H \tag{11}$$

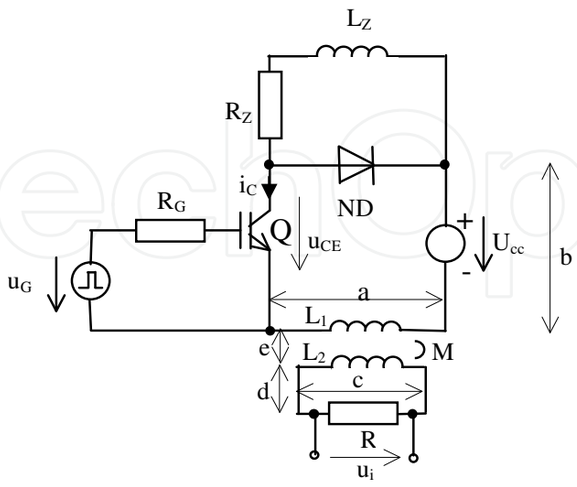

Fig. 5. Investigated circuit

The mutual inductance M calculated from the above mentioned equation is M = 477.4 nH. The magnetic coupling coefficient k is given as

$$k = \frac{M}{\sqrt{L_1 + L_2}} = 0.774 \tag{12}$$

Simulation results are shown in Fig. 6. Results obtained with measurements are shown in Fig. 7 and switching details in Fig. 8.

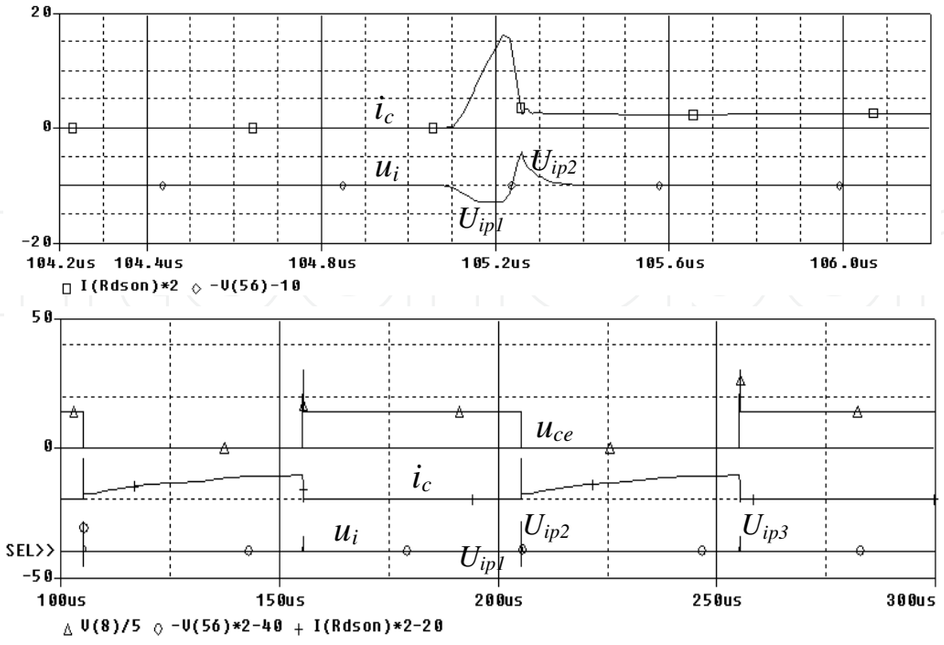

Fig. 6. Simulation results

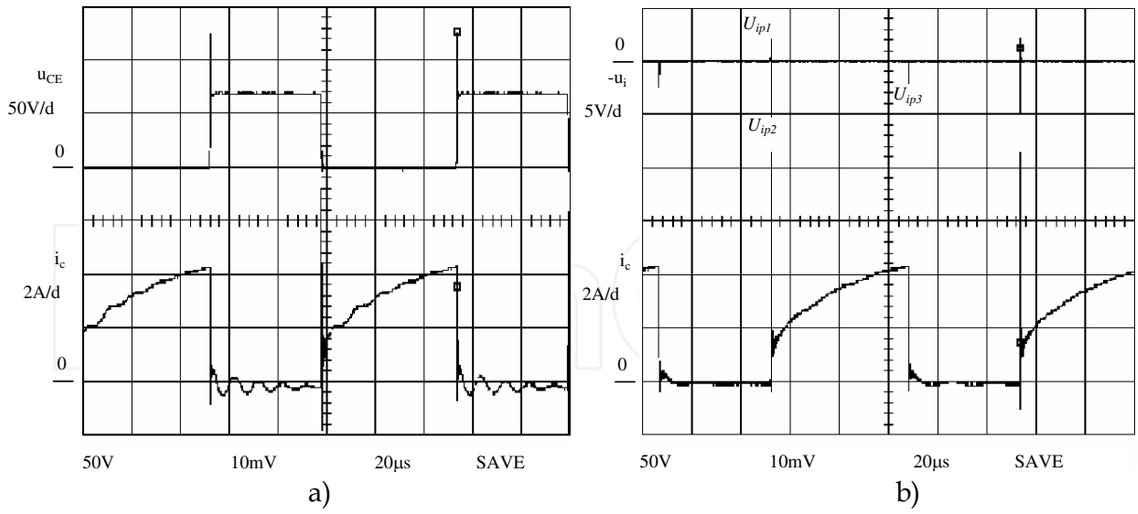

Fig. 7. Measured courses a) voltage u_{CE} and current i_C; b) voltage $-u_i$ and current i_C

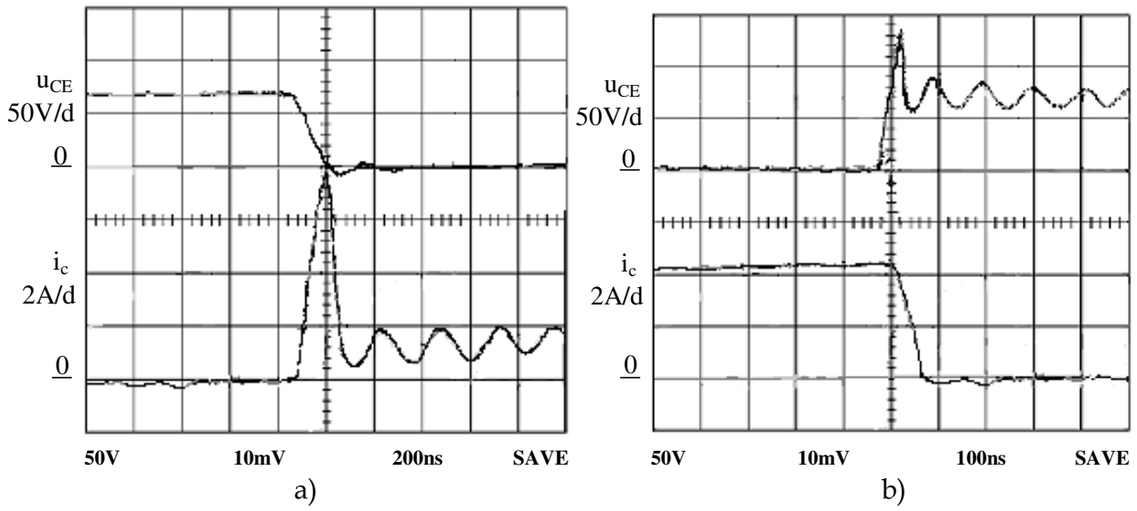

Fig. 8. Details of voltage u_{CE} and current i_C a) switching on state; b) switching off state

A comparison of the simulated and measured results shows that peaks of transistor current *ic* have the same values, i.e. 8.4 A, in both cases. The same values, i.e. 4.4 A, have both the simulated and measured transistor current at the moment when transistor is switched off. There is a small difference only between the simulated and measured curves of the transistor voltage u_{CE}. The overvoltage generated at the transistor switching off reaches the value of 150 V for the simulated result. However, the corresponding overvoltage has only the value of 130 V for the measured result. Peaks of the simulated and measured induced voltages have the same values of U_{i1} = -2.2 V, U_{i2} = 5.02 V, U_{i1} = 2.1 V. This means that such method is acceptable for inductive coupling investigation of the EMC problem.

4. Capacitive coupling

The capacitive coupling is typical for galvanically separated circuit nodes among which the mutual influence is represented by electric field strength $\overline{E}$. Its distribution is given by the

potential at the particular nodes, geometry of the system and dielectric properties of materials and media involved (Fig. 9).

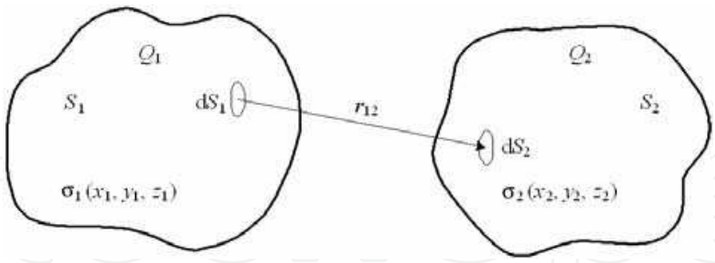

Fig. 9. Capacitive coupling

For the predictive investigation of the capacitive couplings we will start from the well-known Maxwell equation modified for electrostatic field

$$\text{rot}\,\bar{E} = 0. \tag{13}$$

The vector of electric field strength generated by the first electrode at any external point $\bar{r}_0$ is

$$\bar{E}_1 = \frac{1}{4\pi\varepsilon_0}\int_{S_1}\frac{\bar{r}_{10}}{r_{10}^3}.\sigma_1 dS, \tag{14}$$

where S_1 is electrode surface and σ_1 is its surface density calculated by ratio $\sigma_1 = Q_1/S_1$. The total vector $\bar{E}$ at point $\bar{r}_0$ of the system is then given as the sum of vectors $\bar{E}_1$ and $\bar{E}_2$ induced by both charged surfaces. The value of voltage between the electrodes follows from equation

$$U_{12} = \varphi_1 - \varphi_2 = \int_1^2 (\bar{E}_1 + \bar{E}_2).d\bar{r}_{12} = \frac{1}{4\pi\varepsilon_0}\int_1^2\left(\int_{S_1}\frac{\bar{r}_{10}}{r_{10}^3}.\sigma_1 dS + \int_{S_2}\frac{\bar{r}_{20}}{r_{20}^3}.\sigma_2 dS\right)d\bar{r}_{12} \tag{15}$$

where r_{12} is the distance between two elementary parts of the surfaces dS_1 and dS_2. If we suppose that $Q_1 = Q$ and $Q_2 = -Q$, then the capacitance of the system may be expressed by equation

$$C_{12} = Q / U_{12} \tag{16}$$

Often the engineers must determine the mutual parasitic capacitance of two wires of general geometry, as is shown in Fig. 10. In such cases the analytical expression for the resultant capacitance is either very complicated or does not exist at all and the only way how to find its value is to use an appropriate numerical procedure. But its application often requires introduction of suitable simplifying assumptions.

Consider an arrangement of two massive conductors with homogeneous charges Q and $-Q$. Both conductors are of cylindrical shape whose radii are R_1 and R_2, respectively, while their lengths are l_1 and l_2. Let us divide them into thin slices whose thicknesses are in turn Δl_{1i}, $i = 1, m$ and Δl_{2j} $j = 1, n$, so that $l_1 = \sum_{i=1}^{m}\Delta l_{1i}$, $\quad l_2 = \sum_{j=1}^{n}\Delta l_{2j}$.

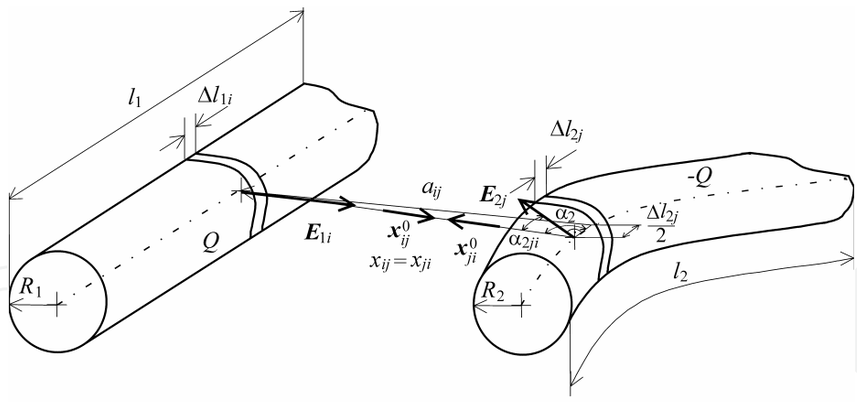

Fig. 10. Capacitive coupling

The potential of the second conductor can be expressed by formula

$$\varphi_2 = \sum_{j=1}^{n}\sum_{i=1}^{m}\left(\int_{R_2}^{\infty}\bar{E}_{2j}.d\bar{x}_{ji} + \int_{x_{ij}-R_2}^{\infty}\bar{E}_{1i}.d\bar{x}_{ij}\right) = \sum_{j=1}^{n}\sum_{i=1}^{m}\left(\int_{R_2}^{\infty}\frac{-Q.\bar{x}_{ji}^0}{2\pi\varepsilon\Delta l_{2j}x}.d\bar{x}_{ji} + \int_{x_{ij}-R_2}^{\infty}\frac{Q.\bar{x}_{ij}^0}{2\pi\varepsilon\Delta l_{1i}x}.d\bar{x}_{ij}\right) =$$
$$= \frac{Q}{2\pi\varepsilon}\sum_{j=1}^{n}\sum_{i=1}^{m}\left(\frac{\ln R_2}{\Delta l_{2j}}\cos\alpha_{\boldsymbol{E}_{2j}\boldsymbol{x}_{ji}^0} - \frac{\ln\left(x_{ij}-R_2\right)}{\Delta l_{1i}}\cos\alpha_{\boldsymbol{E}_{1i}\boldsymbol{x}_{ij}^0}\right). \tag{17}$$

However for correct calculation we have to take only such members of *i* series for which is valid fact that its vectors $\bar{E}_{1i}$ and $d\bar{x}_{ij}$ are collinear, so only such which fulfill the condition

$$\cos\alpha_{\boldsymbol{E}_{1i}\boldsymbol{x}_{ij}^0} = \cos\alpha_{1ij} = 1 \tag{18}$$

The expression $\cos\alpha_{\boldsymbol{E}_{2j}\boldsymbol{x}_{ji}^0} = \cos\alpha_{2ji}$ is possible to derive from Fig. 10. as final equation:

$$\cos\alpha_{2ji} = \sqrt{1-\left(\frac{x_{ij}^2 + 0.25\Delta l_{2j}{}^2 - a_{ij}^2}{x_{ij}.\Delta l_{2j}}\right)^2} \tag{19}$$

Analogously, it is possible to obtain the potential of the first conductor.
The voltage between both conductors is

$$U_{12} = \varphi_1 - \varphi_2 = \frac{Q}{2\pi\varepsilon}\sum_{i=1}^{m}\sum_{j=1}^{n}\left(\frac{\cos\alpha_{\boldsymbol{E}_{1i}\boldsymbol{x}_{ij}^0}}{\Delta l_{1i}}.\ln\frac{\left(x_{ij}-R_2\right)}{R_1} + \frac{\cos\alpha_{\boldsymbol{E}_{2j}\boldsymbol{x}_{ji}^0}}{\Delta l_{2j}}.\ln\frac{\left(x_{ji}-R_1\right)}{R_2}\right). \tag{20}$$

Now it is possible to express the value of parasitic capacitance using the formula

$$C_{12} = \frac{2\pi\varepsilon}{\sum_{i=1}^{m}\sum_{j=1}^{n}\left(\frac{\cos\alpha_{\boldsymbol{E}_{1i}\boldsymbol{x}_{ij}^0}}{\Delta l_{1i}}.\ln\frac{\left(x_{ij}-R_2\right)}{R_1} + \frac{\cos\alpha_{\boldsymbol{E}_{2j}\boldsymbol{x}_{ji}^0}}{\Delta l_{2j}}.\ln\frac{\left(x_{ji}-R_1\right)}{R_2}\right)}. \tag{21}$$

The verification of correctness of the obtained results can be carried out by simulation and measurements. For this purpose, it is possible to use the connection of a DC impulse converter shown in Fig. 11.

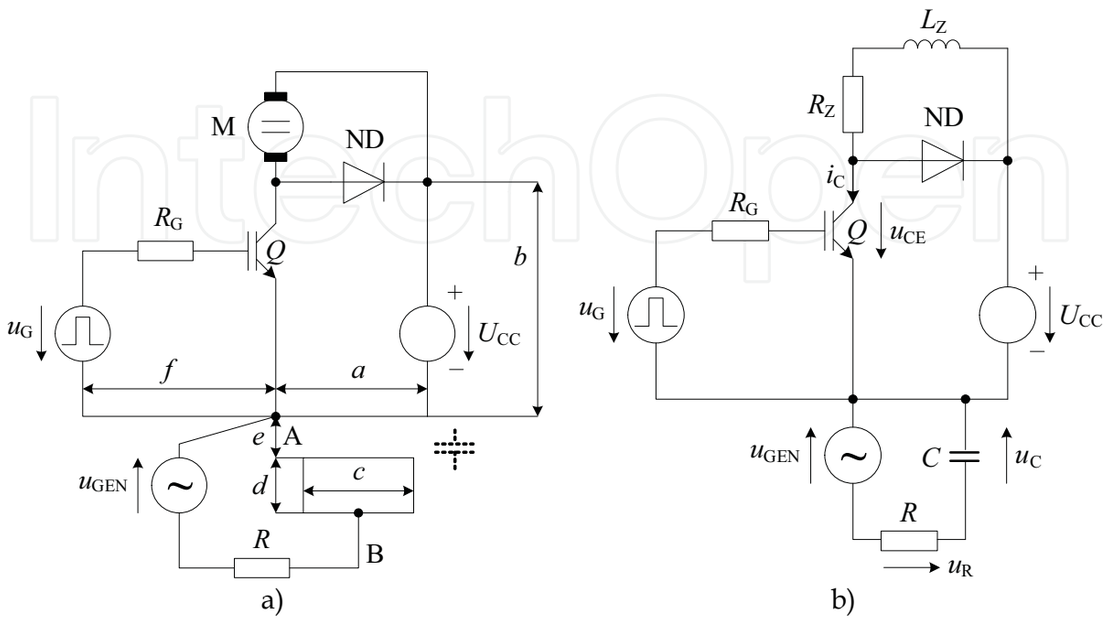

Fig. 11. Investigated circuit a) measured; b) simulated

Now we will determine the value of the parasitic capacitance between the node A of impulse converter and node B of the sense loop. The ambient dielectric is air. The geometrical dimensions of the investigated circuits are $a = f = 0.2$ m, $b = 0.3$ m, $c = 0.1$ m, $d = 0.05$ m, $e = 0.00135$ m. The conductors are made of copper, with radius $R = 0.0006$ m. From the above parameters and figure Fig. 12 it is possible to calculate the individual partial parasitic capacitances

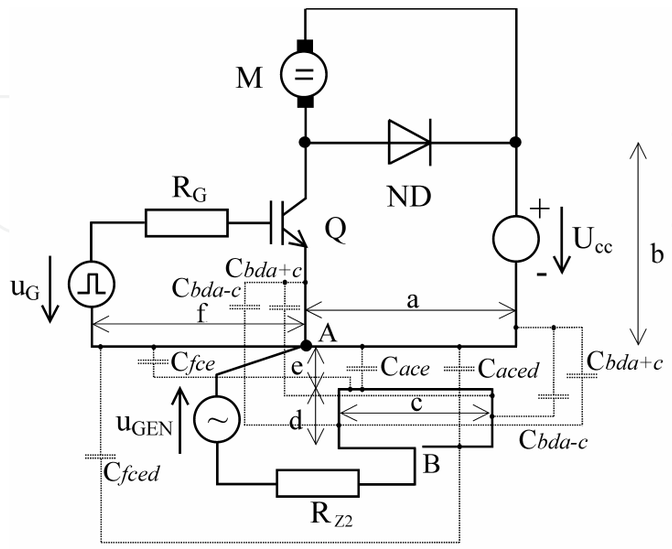

Fig. 12. Detailed expression of main parasitic capacitancies

Based on equation (21) and Fig. 12 the individual circuit capacitances are C_{ace} = 16.629 pF, C_{aced} = 0.8306 pF, C_{fce} = 0.6391 pF, C_{fced} = 0.6314 pF, $C_{bda\text{-}c}$ = 0.3989 pF, C_{bda+c} = 0.3658 pF, $C = C_{ace} + C_{aced} + C_{fce} + C_{fced} + 2\,C_{bda\text{-}c} + 2\,C_{bda+c}$ = 20.26 pF.
Now, it is possible to realize the simulation analysis in the PSPICE program. The connection of the simulated circuit is shown in Fig. 11. The parameters of the individual elements are U_{CC} = 70 V, R_Z = 11.66 Ω, L_Z = 400 μH, R_{Z2} = 1 MΩ, u_{GEN} = 2sin (ωt) V. The simulation results for frequencies f = 10 kHz and f = 50 kHz are depicted in Fig. 13.

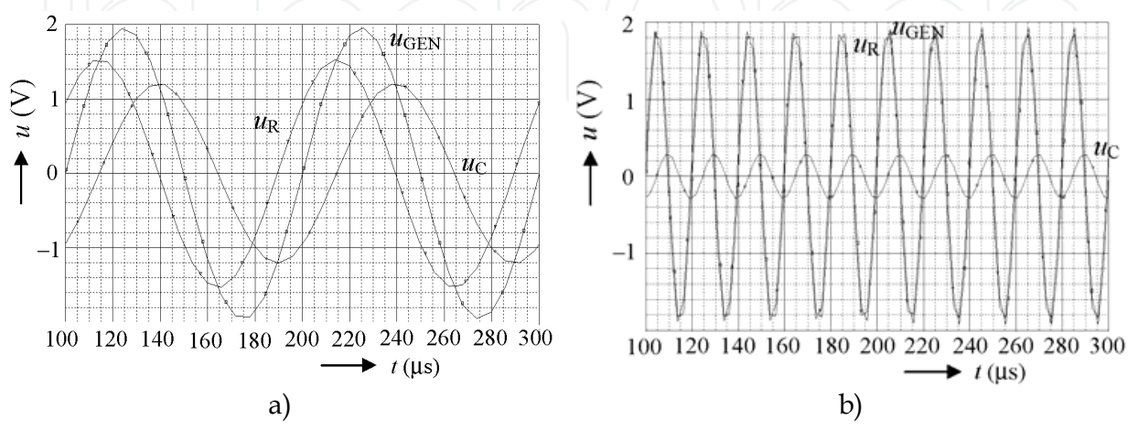

Fig. 13. Simulation results for frequency a) f = 10 kHz; b) f = 50 kHz

The measured values of u_{CE}, $u_{GEN,}$ and u_C are shown in Fig. 14.
The comparison of the simulated and measured results shows that the results are identical. This coincidence leads to the conclusion that the derived analytical formula for parasitic capacitance is correct.
The presented analysis indicates that not only the high current switching frequencies have the main influence on the EMC of the converter, but also their switch-off state with small parasitic resonant load current is equally important.
Although such converter capacitances seem to be negligible, the above analysis shows that they may be of crucial influence. One case occurs when the switching frequency is high, another when the node belongs to the circuit with high impedance. This is obvious for the capacitive coupling between CMOS integrated circuits and power converter circuit, when the EMC aspects can be vital for correct operation of the equipment (Clayton, 1992).

5. Galvanic coupling

The problem of galvanic coupling deals with individual electric equipment or their part's interconnections in such a way, that minimum one or (in some cases as for example feeding net) more common conductors, interconnecting these equipments and so mutual influence is generated.
The working frequencies and the length of common conductor must be taken always into account. In all cases of the galvanic coupling, the fact that electrical components are not ideal and so they are containing certain parasitic capacitances, inductances and real resistances, is valid. Due to higher working frequency of currents flowed by the common conductors, they must be taken as circuits with distributed parameters, during the process of predictive result galvanic coupling investigation. If the working frequencies will be lower, then the interconnecting circuits can be taken as circuits with concentrated parameters.

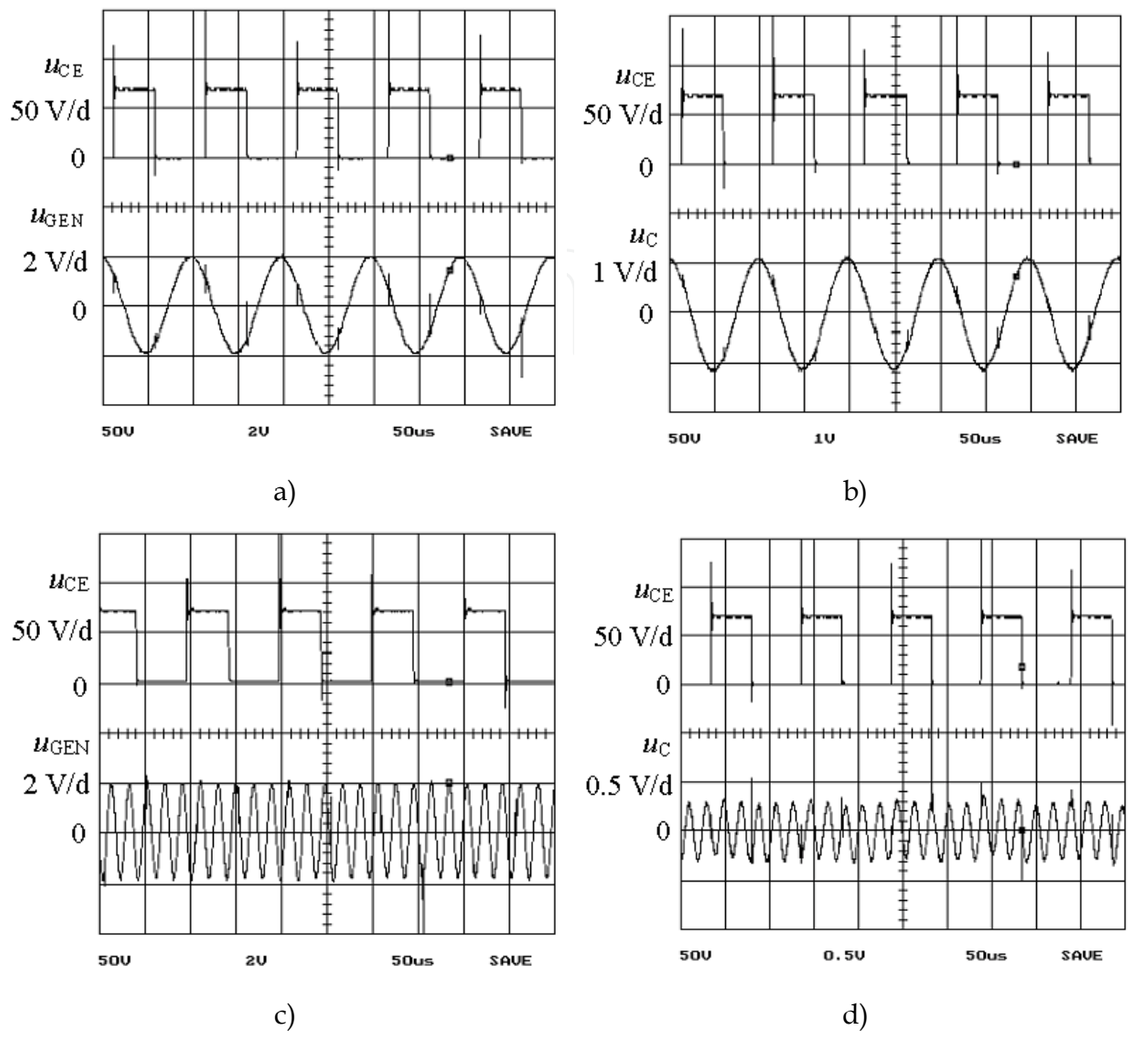

Fig. 14. Measured voltages a) u_{CE} and u_{GEN}; b) u_{CE} and u_C for frequency f = 10 kHz; c) u_{CE} and u_{GEN}; d) u_{CE} and u_C for frequency f = 50 kHz

5.1 Solution for the low frequencies and concentrated parameters

Minimum two or more electric circuits, which are mutually galvanically interconnected by one common conductor with its length l, represent a type of galvanic coupling. Due to low frequency operation it is possible to define the common conductor electrical parameters by concentrated parameters of its resistance R and inductance L. If we suppose in the next step, that the conductor will be made of copper, so the voltage drop on its resistance R will be much smaller in comparison with the voltage drop across its inductance L, which is caused by the time depending change of current. So, for the simplified analysis of the problem the conductor resistance will be neglected in the following. The schematic representation of the described problem is shown in the following figure Fig. 15.

The mathematical description of the situation in the investigated circuit (Fig. 15. a) is then given by the next system of integral-differential equations (if the load created by serial connection of R_1, L_1 and C_1 components is supposed):

$$
\begin{aligned}
u_1 - u_L - u_2 &= u_1 - L.\frac{di_3}{dt} - \left(R_1.i_1 + L_1.\frac{di_1}{dt} + \frac{1}{C_1}.\int i_1.dt \right) = 0 \\
u_{1'} - u_L - u_{2'} &= u_{1'} - L.\frac{di_3}{dt} - \left(R_{1'}.i_{1'} + L_{1'}.\frac{di_{1'}}{dt} + \frac{1}{C_{1'}}.\int i_{1'}.dt \right) = 0 \\
u_{1^k} - u_L - u_{2^k} &= u_{1^k} - L.\frac{di_3}{dt} - \left(R_{1^k}.i_{1^k} + L_{1^k}.\frac{di_{1^k}}{dt} + \frac{1}{C_{1^k}}.\int i_{1^k}.dt \right) = 0 \\
i_3 &= i_1 + i_{1'} + \sum_{k=''}^{n} i_{1^k}
\end{aligned}
\tag{22}
$$

where n is the number of all different loops, contained in the same common conductor. In the case of great number of loops, the analytic investigation of galvanic coupling influence on individual electric circuits is relatively complicated, so it is possible to utilize the available computer numerical simulation programs.

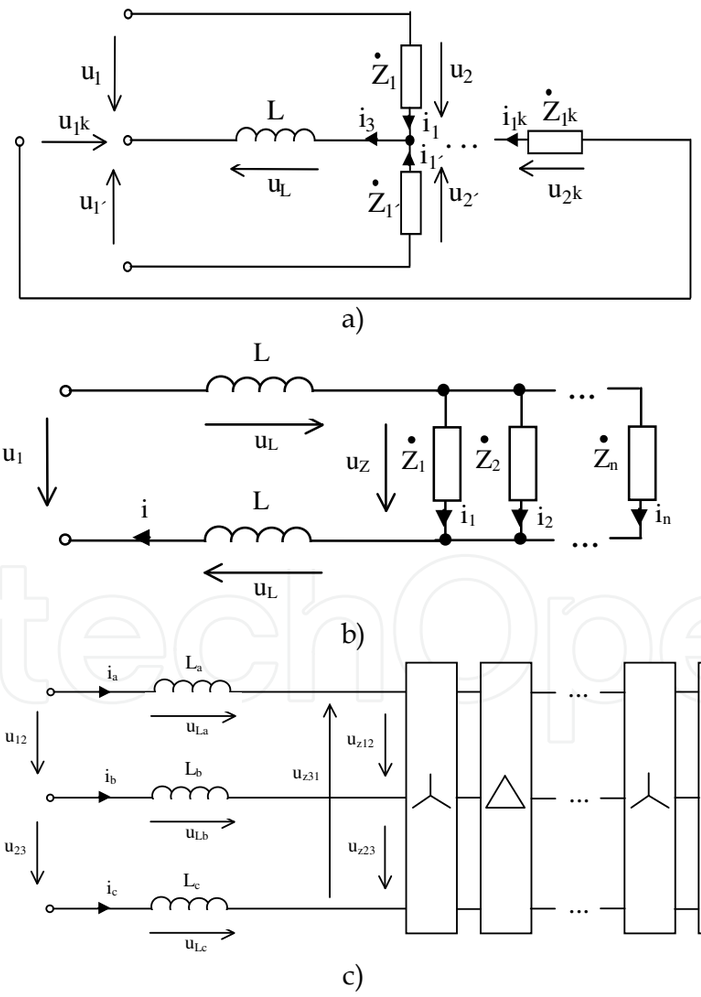

Fig. 15. The schematic representation of the circuit interconnections by a) one common conductor; b) two conductors; c) several common conductors

The multiple interconnection of electrical or electronics circuits realized by two common conductors is typical especially for one phase or DC feeding conductors, as it is shown in figure Fig. 15. b. Due to existence of both the incoming conductor inductances *L*, the total circuit inductance is double. The mutual galvanic coupling is generated at the moment of the optional loop's impedance change. The impedance can be changed up, or down. This situation is typical for the impulse converter circuits, but it is clear that such case occurs also in all other circuits, which use the switching parts.
The interconnection of many electrical or electronic circuits, by several common conductors, is typical for three phase feeding net, as it is shown in figure Fig. 15. c. In case, where four conductors will do those circuits interconnections and also if one of them is a neutral wire, the problem will be the same as the problem of three individual circuits, connected together by only one common conductor. This problem was already described. The circuit can be described by system of equations expressed by a complex vector as:

$$\begin{aligned} \bar{U}_{12} &= j\omega L\bar{I}_1 + (R_1 + j\omega L_1 - j\frac{1}{\omega C_1}).\bar{I}_1 - (R_2 + j\omega L_2 - j\frac{1}{\omega C_2}).\bar{I}_2 - j\omega L\bar{I}_2 \\ \bar{U}_{23} &= j\omega L\bar{I}_2 + (R_2 + j\omega L_2 - j\frac{1}{\omega C_2}).\bar{I}_2 - (R_3 + j\omega L_3 - j\frac{1}{\omega C_3}).\bar{I}_3 - j\omega L\bar{I}_3 \\ \bar{I}_1 + \bar{I}_2 + \bar{I}_3 &= 0 \end{aligned} \tag{23}$$

In the following step, we will try to obtain imagination about the galvanic coupling existence of only two interacting circuits. For the simplification of the analytic investigation it is suitable to suppose, that pure resistors create the loads in both the galvanic connected circuits and that the circuits are in steady states and they are supplied from DC voltage sources as it is shown in figure Fig. 16.
Consider the jump change of supplying voltage from value $U_{1'}$ to zero supposed in lower circuit and no change of supplying voltage or load in the upper circuit. The time dependence description of the voltage u_2 can be obtained by equation

$$u_2 = U_1 - u_L = U_1 - L.\frac{di_3}{dt} = U_1 + U_{1'}.\frac{R_1}{(R_1 + R_{1'})}.e^{-\frac{R_1 R_{1'}}{L(R_1 + R_{1'})}.t} \tag{24}$$

From the obtained relation it is clear, that the first circuit load voltage is changed about value $(U_{1'}.R_1)/(R_1+R_{1'})$ due to existence of the change inside the circuit, which is galvanically connected with the previous one. No working activity of the first circuit was done and so its switch on steady state remains. In dependence on the load resistor values ratio the voltage drop can be within the open interval $(0,U_{1'})$.
If the supply voltage switching on state inside the second circuit will be investigated, the information about the voltage load u_2 could be obtained by the similar method.

$$u_2 = U_1 - u_L = U_1 - L.\frac{di_3}{dt} = U_1 - U_{1'}.\frac{R_1}{(R_1 + R_{1'})}.e^{-\frac{R_1 R_{1'}}{L(R_1 + R_{1'})}.t} \tag{25}$$

It is evident, that the load voltage value inside the first circuit, can be changed about the voltage drop within the open interval $(-U_{1'},0)$, again in dependence on load resistor values ratio.

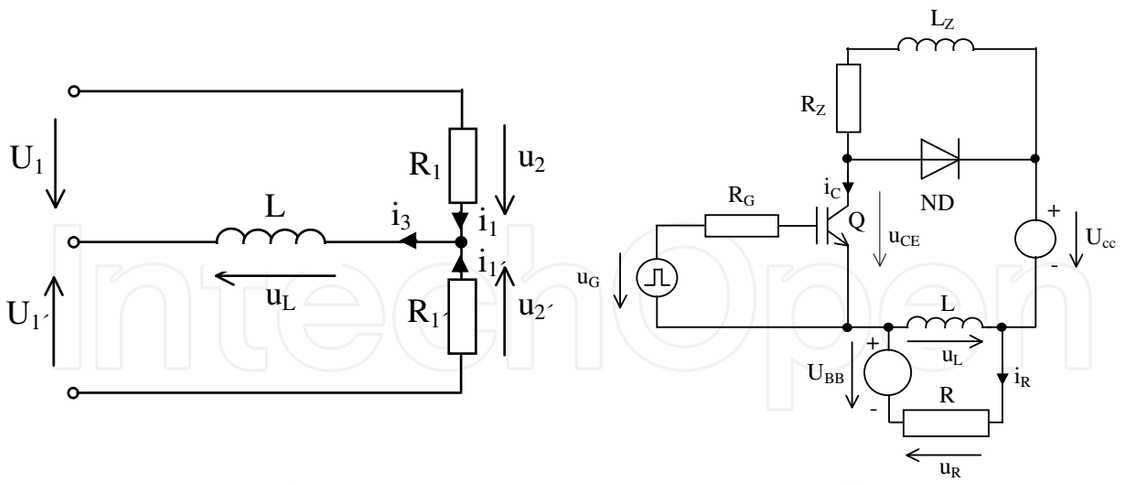

Fig. 16. Electrical scheme of a) the investigated; b) the simulated and measured circuit

Generally, the switching process inside the second circuit is reflected through galvanic coupling to the total possible load voltage u_2 change within the interval range ($-U_{1'}$, $U_{1'}$), depending on load values ratio and the sign of derivation of the current flowed via common conductor inductance L.

The computer numerical simulation realized by the PSPICE program helps us to verify the dependencies obtained analytically. Let the common conductor length be l = 0.1 m. The influence of its magnetic field in distance d = 1 m will be taken into account. The radius of copper conductors is R = 0.6 mm and their relative permeability is μ_r = 0.991. Then inductance L = 302 nH. In the next step will suppose, that voltage $u_{1'}$ has a rectangle shape with the amplitude 70 V, duty factor z = 0.5 and switching frequency f = 10 kHz. The other circuit parameters are $R_{1'}$ = 11.66 Ω, U_1 = 5 V, R_1 = 10 kΩ and L = 302 nH. Based on the derived equations and given parameters, we can calculate the voltage u_2 peaks so, that the time in the equations (24) and (25) will be replaced by t = 0. Then we will obtain:

$$u_2(t_{sw\ off}) = U_1 + U_{1'}.\frac{R_1}{(R_1 + R_{1'})} = 5 + 70.\frac{10000}{10011.66} = 74.918 \text{ V} \tag{26}$$

Analogically it is possible to state the voltage peak of u_2 at the moment of the second circuit switch on.

$$u_2(t_{sw\ on}) = U_1 - U_{1'}.\frac{R_1}{(R_1 + R_{1'})} = 5 - 70.\frac{10000}{10011.66} = -64.918 \text{ V} \tag{27}$$

The courses of the input voltages u_1 and $u_{1'}$, the load voltages u_2 and $u_{2'}$ and the voltage u_L are introduced in figure Fig. 17. All data were obtained by computer circuit simulation in the PSPICE program for given circuit parameters. The coincidence of the results obtained analytically as equations derived in the previous parts and by computer numerical simulation is evident, at the first sight.

Let the derived results verification be done by simulation and practical measuring of the power semiconductor converter circuit connected according to the scheme shown in figure Fig. 16b (Tihanyi, 1995). The circuit parameters are: U_{CC} = 70 V, R_Z = 11.66 Ω, L_Z = 400 μH,

L = 302 nH, R = 10 kΩ, U_{BB} = 5 V. The power IGBT transistor is switching with the frequency of 10 kHz and the duty cycle z = 0.5.

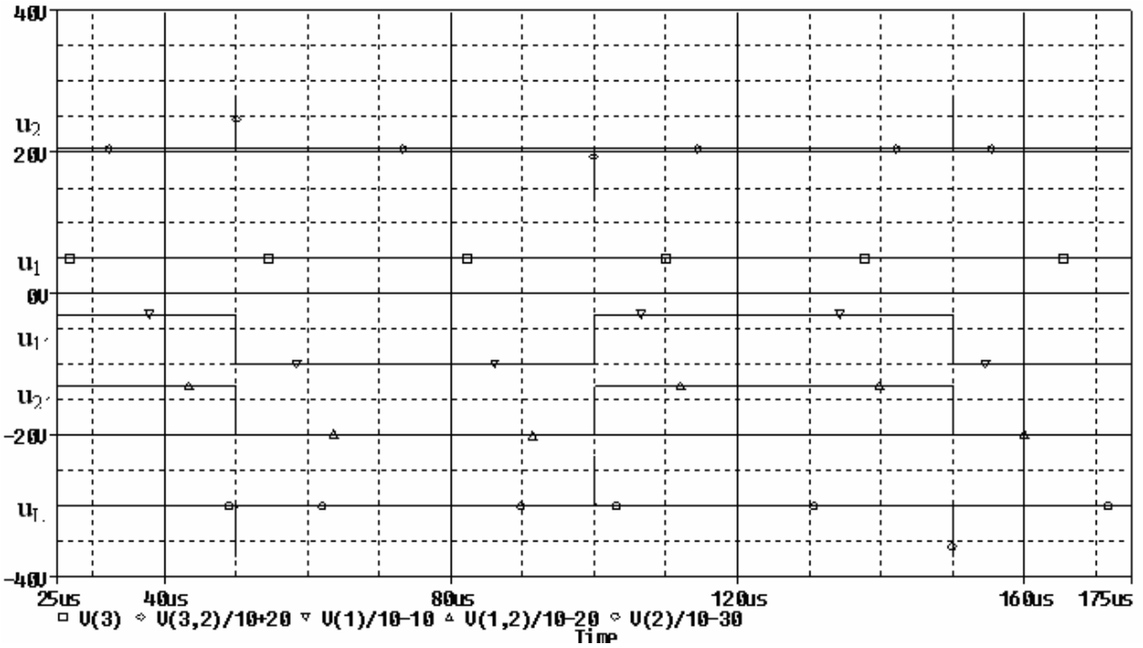

Fig. 17. Results obtained by simulation in the PSPICE program

The courses of the transistor voltage u_{CE}, inductance voltage u_L and resistance R voltage u_R obtained by simulation for the frequency f = 10 kHz are depicted in figure Fig. 18a.

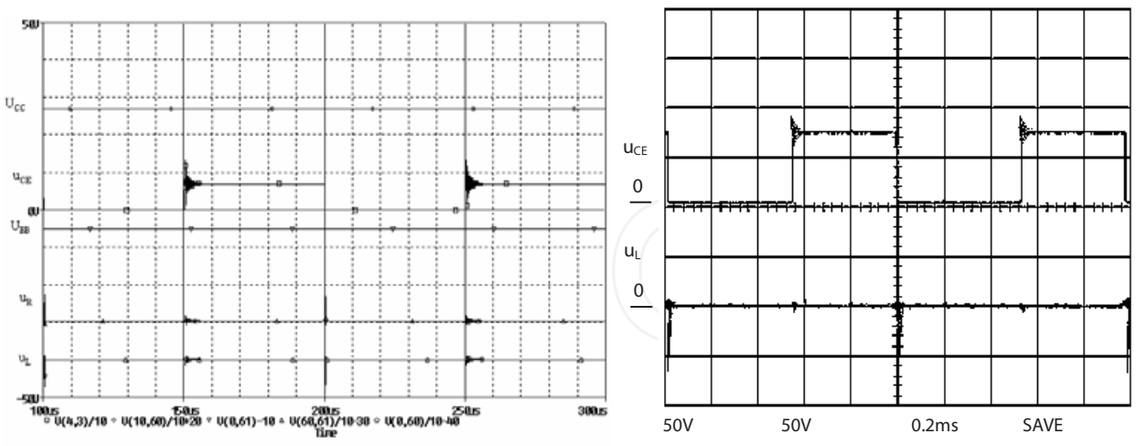

a) b)

Fig. 18. The results obtained by a) simulation in the PSPICE program; b) measurement

In this case the voltage jump does not exist, because the transistor is switching by a finite velocity. On the basis of this fact, the switching inductance voltage drop reaches the values of approximately ±10 V in dependence on the current's rising or falling slope. The most expressive inductance voltage drop appears at the moment of the transistor current falling, caused by the existence of the charge of commutation diode. This time, the current slope is

markedly increasing, and so the parasitic inductance voltage drop is increasing too. Comparable results, obtained by the verification measurement, are displayed in figure Fig. 18b. The coincidence with the simulation results is evident.

5.2 Solution for the higher frequencies and distributed parameters

The mutual interconnection of electric circuits by two common conductors with the length *l* (the length is long or the transferred signal has high frequency) represents the investigation problem of a line with distributed parameters (in the following ″long transmission line″ or ″long line″ only). The basic representation of such electric circuit interconnection is drawn in figure Fig. 19.

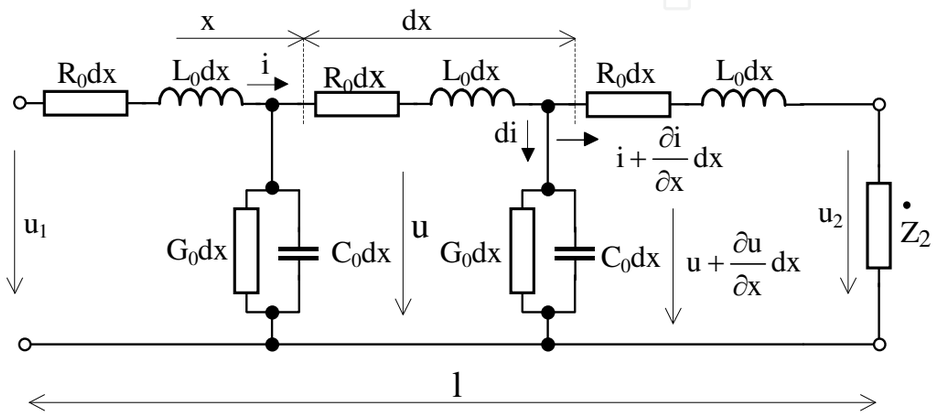

Fig. 19. The equivalent scheme of long transmission line with distributed parameters

It is known from the electric circuit theory that the time dependence investigation of line voltage or current, at optional line position, leads to the system solution of two partial-differential equations.

In that case an input voltage and a current of long transmission line it is possible to describe by time harmonic functions in the form,

$$u = U_m \sin(\omega t + \psi_u) \quad \Rightarrow \bar{U} e^{j\omega t} \tag{28}$$

$$i = I_m \sin(\omega t + \psi_i) \quad \Rightarrow \bar{I} e^{j\omega t} \tag{29}$$

the resulting solution of the given equation system, expressed by complex voltage and current vectors, will be given as:

$$\bar{U} = \bar{U}_1 ch\, \bar{\gamma} x - \bar{Z}_v \bar{I}_1 sh\, \bar{\gamma} x \tag{30}$$

$$\bar{I} = \bar{I}_1 ch\, \bar{\gamma} x - \frac{\bar{U}_1}{\bar{Z}_v} sh\, \bar{\gamma} x \tag{31}$$

where

$$\bar{\gamma} = \beta + j\alpha = \sqrt{\left(R_0 + j\omega L_0\right)\left(G_0 + j\omega C_0\right)} \tag{32}$$

$$\beta = \sqrt{\frac{1}{2}\left[\sqrt{\left(R_0^2 + \omega^2 L_0^2\right)\left(G_0^2 + \omega^2 C_0^2\right)} + R_0 G_0 - \omega^2 L_0 C_0\right]} \tag{33}$$

$$\alpha = \sqrt{\frac{1}{2}\left[\sqrt{\left(R_0^2 + \omega^2 L_0^2\right)\left(G_0^2 + \omega^2 C_0^2\right)} - R_0 G_0 + \omega^2 L_0 C_0\right]} \tag{34}$$

$$\overline{Z}_v = \sqrt{\frac{\left(R_0 + j\omega L_0\right)}{\left(G_0 + j\omega C_0\right)}} = Z_v . e^{j\varphi_v} \tag{35}$$

In the field of power electronics a non-harmonic unipolar or bipolar signal is utilized many times for indirect converters. To enable a given problem's mathematical analysis, the non-harmonic signal must be described by the system of harmonic functions.
The expression of the investigated voltage dependence will be done by calculated coefficients of Fourier's series and by the next equation.

$$u(t) = \sum_{k=0}^{\infty} \left(a_k . \cos(k\omega t) + b_k \sin(k\omega t)\right) \tag{36}$$

where: $a_0 = \frac{1}{T}\int_0^T f(\omega t)dt$, $a_k = \frac{2}{T}\int_0^T f(\omega t).cos(k\omega t)dt$, $b_k = \frac{2}{T}\int_0^T f(\omega t).sin(k\omega t)dt$.

For a long line galvanic coupling influence investigation, it is necessary to obtain the time dependence of the voltage at the end of the long transmission line. It is possible to calculate the searched voltage on the basis of an equation expressing the time voltage dependence at an optional position of a long transmission line, which is far-away from the beginning of the line about the distance x so, that this length will be replaced by the line length l and the complex current vector $\overline{I}_1$ will be replaced by the relation $\overline{U}_1 / \overline{Z}_{input}$. Let the feeding voltage have square-wave shape with the amplitude U_1 .

$$\overline{U}_2 = \frac{U_1}{2}.\left(\left(e^{(\beta l + j(\alpha l + \varphi_U))} + e^{-(\beta l + j(\alpha l - \varphi_U))}\right) - \frac{a + jb}{c + jd}.\left(e^{(\beta l + j(\alpha l + \varphi_U))} - e^{-(\beta l + j(\alpha l - \varphi_U))}\right)\right) \tag{37}$$

where the expressions a, b, c, d are calculated on the basis of following equations:

$$a = Z_2 . e^{\beta l}.\cos(\alpha l + \varphi_{Z2}) - Z_2 . e^{-\beta l}.\cos(\varphi_{Z2} - \alpha l) + Z_v . e^{\beta l}.\cos(\alpha l + \varphi_{Zv}) + Z_v . e^{-\beta l}.\cos(\varphi_{Zv} - \alpha l) \tag{38}$$

$$b = Z_2 . e^{\beta l}.\sin(\alpha l + \varphi_{Z2}) - Z_2 . e^{-\beta l}.\sin(\varphi_{Z2} - \alpha l) + Z_v . e^{\beta l}.\sin(\alpha l + \varphi_{Zv}) + Z_v . e^{-\beta l}.\sin(\varphi_{Zv} - \alpha l) \tag{39}$$

$$c = Z_2 . e^{\beta l}.\cos(\alpha l + \varphi_{Z2}) + Z_2 . e^{-\beta l}.\cos(\varphi_{Z2} - \alpha l) + Z_v . e^{\beta l}.\cos(\alpha l + \varphi_{Zv}) - Z_v . e^{-\beta l}.\cos(\varphi_{Zv} - \alpha l) \tag{40}$$

$$d = Z_2 . e^{\beta l}.\sin(\alpha l + \varphi_{Z2}) + Z_2 . e^{-\beta l}.\sin(\varphi_{Z2} - \alpha l) + Z_v . e^{\beta l}.\sin(\alpha l + \varphi_{Zv}) - Z_v . e^{-\beta l}.\sin(\varphi_{Zv} - \alpha l) \tag{41}$$

The electric circuits interconnection realized by one common conductor with the distributed parameters, is a special case, where more electric circuits are utilizing one common conductor, which is either long or serves for high frequency signal conduction.

The problem analysis will be done for the case of two electric circuits interconnection, the scheme of which is shown in figure Fig. 20. Let the upper circuit be supplied by a DC

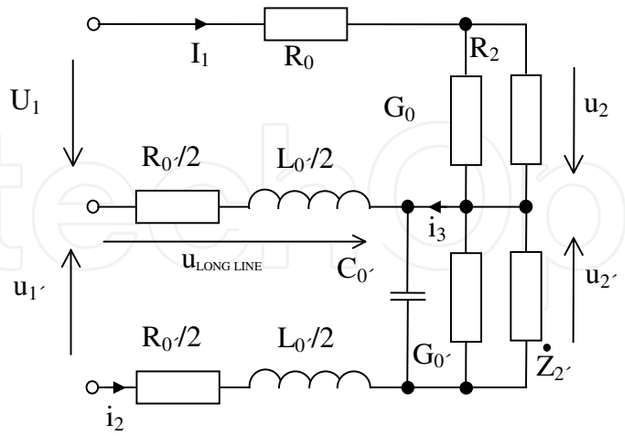

Fig. 20. The scheme of investigated circuit connection

voltage source with the value U_1 = 5 V. As interface conductor the same cable as in the previous case was used, it means a CYSY 4x1.5 mm² with the length 15m and with parameters $R_{0´}$ = 0.047 Ω/m, $L_{0´}$ = 343 nH/m, $G_{0´}$ = 33.3 μS/m, $C_{0´}$ = 118 pF/m.

The upper circuit has no signal change. The output voltage u_2 should be reflecting only the voltage drops caused by long line longitudinal resistance and a vertical drop-in. Let the lower circuit be supplied by the same periodical impulse signal $u_{1´}$ as in the case of the previous analysis. It is possible to state the mutual circuit galvanic coupling influence by finding the upper circuit real voltage u_2 course. According to the 2nd Kirchoff's law, we can write the equation for the investigated circuit:

$$u_2 = U_1 - u_{1´} + u_{2´} - R_0.I_1 = U_1 - u_{1´} + u_{2´} - R_0.\frac{U_1}{\frac{R_2.G_0}{R_2+G_0} + R_0} \tag{42}$$

The analytical form for the voltages $u_{1´}$ and $u_{2´}$ the description can be obtained, from the previous analysis, as equations for input and output voltages of long transmission line. By the substitution of these voltages, the searched relation for time dependence of the voltage u_2 is possible to receive. Any accessible Excel program will do the graphical interpretation of the resulting solution again, figures Fig. 21.

Equally, as in the previous case a multiple verification of correctness can be done by the PSPICE program simulation (Fig. 22) and by practical measurement (Fig. 23).

The coincidence of the obtained results is evident. Small differences concerning the input and output voltage oscillation damping are given by the fact, that for the input and output voltages the infinite Fourier's series were replaced by only the first 40 components in the Excel program.

Very often a symmetrical three-phase load is connected to the inverter impulse output, with the frequency of few tenths of kHz, by the cable with the length within the range 3 up to 20m during the practical use of power semiconductor converters. This case represents the interconnection of two circuits, by a long line with the distributed parameters in the three phases connection.

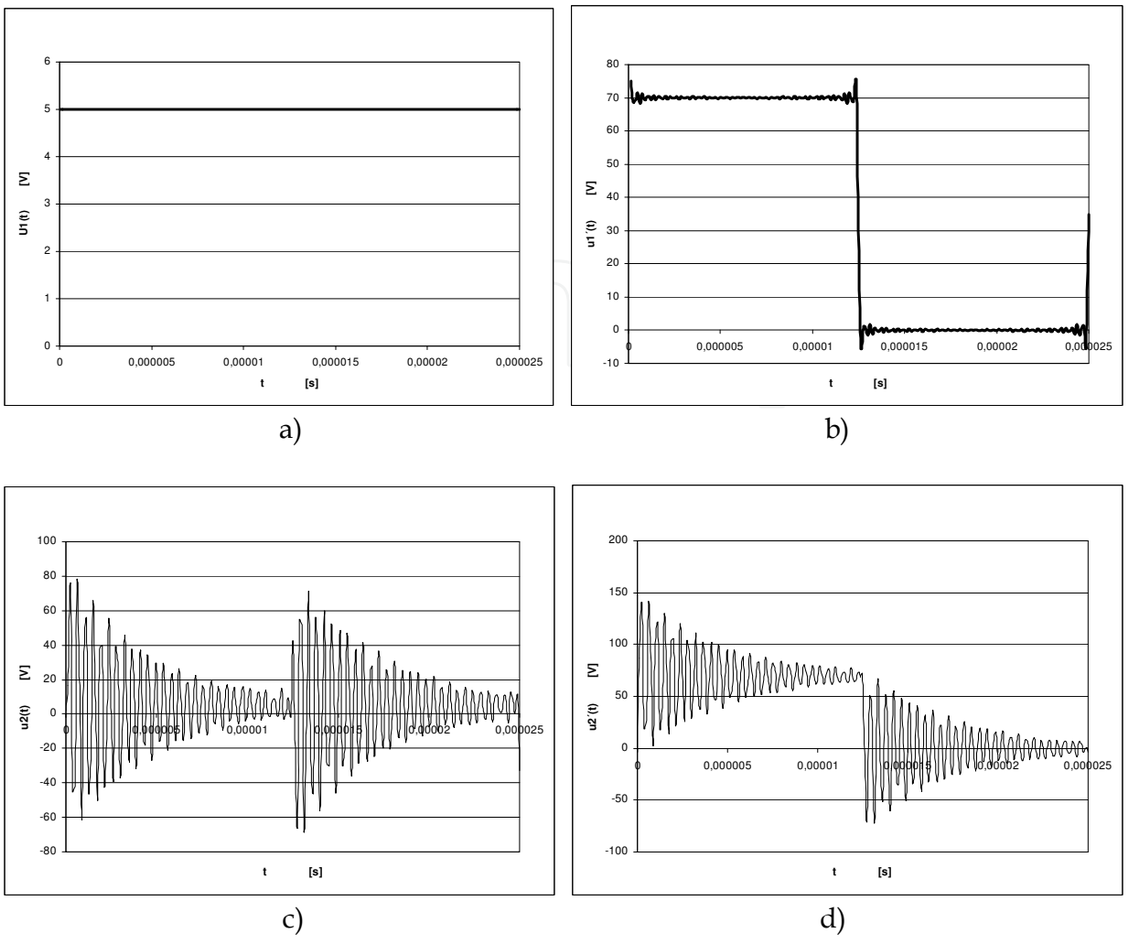

a) b)

c) d)

Fig. 21. Theoretical results a) input voltage $U_{1,}$ b) input voltage $u_{1'}$; c) output voltage u_2; d) output voltage $u_{2'}$

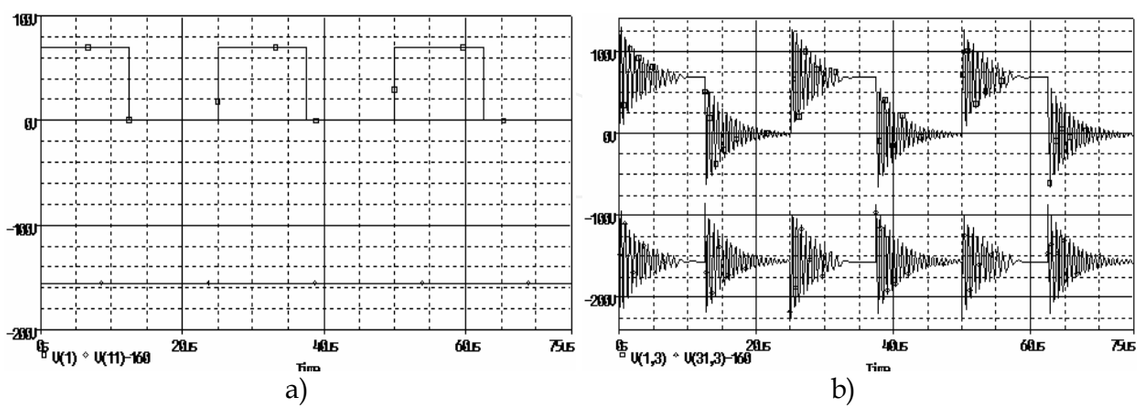

a) b)

Fig. 22. Simulated results a) input voltages $u_{1'}$ and U_1; b) output voltages $u_{2'}$ and u_2

Let the galvanic coupling investigation of such circuit topology be done by a temporal dependence calculation of the voltages $u_{12'}$, $u_{23'}$ and $u_{31'}$ at the end position of a long transmission line. The input long line voltages are graphically depicted in figure Fig. 24.

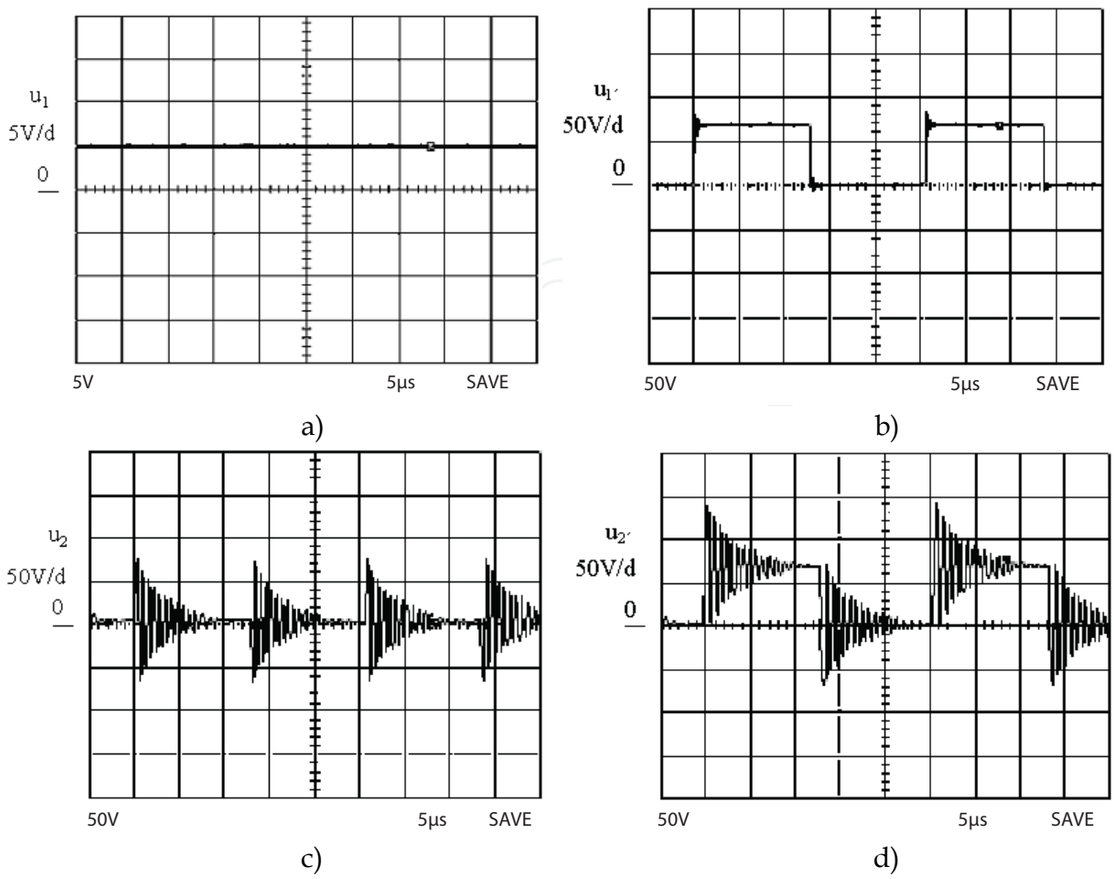

Fig. 23. Measured results a) input voltages u_1; b) input voltages u_1; c) output voltage u_2; d) output voltage $u_{2'}$

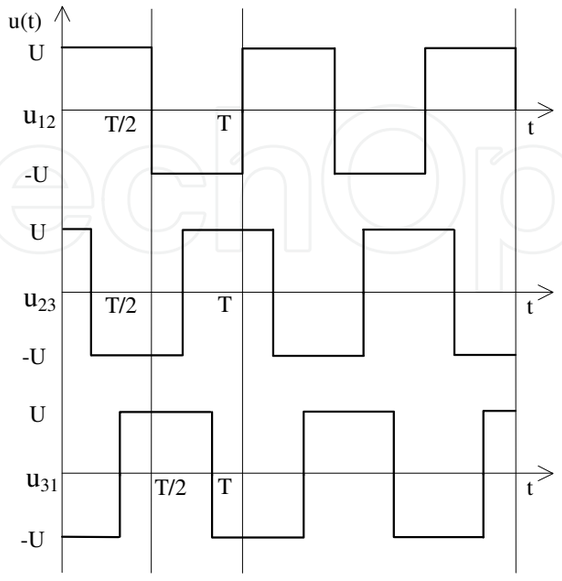

Fig. 24. The input voltages u_{12} , u_{23} and u_{31}

The amplitudes of the input voltages are U = 400 V. The same interconnecting cable was used as in the previous case with the parameters: CYSY 4x1.5 mm², with the length 15m, R_0 = 0.047 Ω/m, L_0 = 343 nH/m, G_0 = 33.3 μS/m, C_0 = 118 pF/m. The load is symmetrical, resistive-inductive with parameters R_2 = 10 Ω, L_2 = 1 mH. For the calculation of the output voltages $u_{12'}$, $u_{23'}$ and $u_{31'}$ can be used the relations derived in previous analyses, but it is necessary to express the non-harmonic input feeding voltages of the long transmission line by a harmonic functions. The Fourier's series will be used again.

$$u_{12}(t) = \frac{4U}{\pi}\sin(\omega t) + \frac{4U}{3\pi}\sin(3\omega t) + \frac{4U}{5\pi}\sin(5\omega t) + \ldots = \sum_{k=0}^{\infty}\frac{4U}{(2k+1)\pi}\sin((2k+1)\omega t) \tag{43}$$

$$u_{23}(t) = \frac{4U}{\pi}\sin(\omega(t-\frac{T}{3})) + \frac{4U}{3\pi}\sin(3\omega(t-\frac{T}{3})) + \frac{4U}{5\pi}\sin(5\omega(t-\frac{T}{3})) + \ldots = \sum_{k=0}^{\infty}\frac{4U}{(2k+1)\pi}\sin((2k+1)\omega(t-\frac{T}{3})) \tag{44}$$

$$u_{31}(t) = \frac{4U}{\pi}\sin(\omega(t-\frac{2T}{3})) + \frac{4U}{3\pi}\sin(3\omega(t-\frac{2T}{3})) + \frac{4U}{5\pi}\sin(5\omega(t-\frac{2T}{3})) + \ldots = \sum_{k=0}^{\infty}\frac{4U}{(2k+1)\pi}\sin((2k+1)\omega(t-\frac{2T}{3})) \tag{45}$$

If the calculated relations for the input voltages are substituted by the derived equation (37), which describes the temporal dependence of the voltage at the end of the long line and only the imaginary part of the complex solution will be taken into account, because only this part corresponds to the sinusoidal input voltage, thus we can obtain the relations (46) up to (48).

$$u_{12'}(t) = \sum_{k=0}^{\infty}\frac{2U}{(2k+1)\pi}.(e^{\beta l}.\sin((2k+1)\omega t + \varphi_U + \alpha l) + e^{-\beta l}.\sin((2k+1)\omega t + \varphi_U - \alpha l) - \frac{\sqrt{a^2+b^2}}{\sqrt{c^2+d^2}}.e^{\beta l}. \tag{46}$$
$$.\sin((2k+1)\omega t + \varphi_U + \alpha l + arctg\frac{b}{a} - arctg\frac{d}{c}) + \frac{\sqrt{a^2+b^2}}{\sqrt{c^2+d^2}}.e^{-\beta l}.\sin((2k+1)\omega t + \varphi_U - \alpha l + arctg\frac{b}{a} - arctg\frac{d}{c}))$$

$$u_{23'}(t) = \sum_{k=0}^{\infty}\frac{2U}{(2k+1)\pi}.(e^{\beta l}.\sin((2k+1)\omega(t-\frac{T}{3}) + \varphi_U + \alpha l) + e^{-\beta l}.\sin((2k+1)\omega(t-\frac{T}{3}) + \varphi_U - \alpha l) - \frac{\sqrt{a^2+b^2}}{\sqrt{c^2+d^2}}.e^{\beta l}. \tag{47}$$
$$.\sin((2k+1)\omega(t-\frac{T}{3}) + \varphi_U + \alpha l + arctg\frac{b}{a} - arctg\frac{d}{c}) + \frac{\sqrt{a^2+b^2}}{\sqrt{c^2+d^2}}.e^{-\beta l}.\sin((2k+1)\omega(t-\frac{T}{3}) + \varphi_U - \alpha l + arctg\frac{b}{a} - arctg\frac{d}{c}))$$

$$u_{31'}(t) = \sum_{k=0}^{\infty}\frac{2U}{(2k+1)\pi}.(e^{\beta l}.\sin((2k+1)\omega(t-\frac{2T}{3}) + \varphi_U + \alpha l) + e^{-\beta l}.\sin((2k+1)\omega(t-\frac{2T}{3}) + \varphi_U - \alpha l) - \frac{\sqrt{a^2+b^2}}{\sqrt{c^2+d^2}}.e^{\beta l}. \tag{48}$$
$$.\sin((2k+1)\omega(t-\frac{2T}{3}) + \varphi_U + \alpha l + arctg\frac{b}{a} - arctg\frac{d}{c}) + \frac{\sqrt{a^2+b^2}}{\sqrt{c^2+d^2}}.e^{-\beta l}.\sin((2k+1)\omega(t-\frac{2T}{3}) + \varphi_U - \alpha l + arctg\frac{b}{a} - arctg\frac{d}{c}))$$

During the calculation process, the load impedance value recalculation from star to triangle could not be forgotten, because the temporal curves of interline voltages are searched. The Excel program utilized for the first 40 components of Fourier's series will again do the graphical representation of the obtained results. The respective curves are drawn in Fig. 25. The following figure (Fig. 26) shows the sum of all three inputs and output interlines voltages. From the courses, it is evident, that during such a choice of feeding signal shape, the non-harmonic supply system, containing the expressive amount of 3rd harmonic voltage and its multiples, is generated. In the case of four-conductor circuit interconnection, the loop current, flowing via a neutral wire, is created by the resulting potential of the source node, which is in contradiction to the standard requirements.

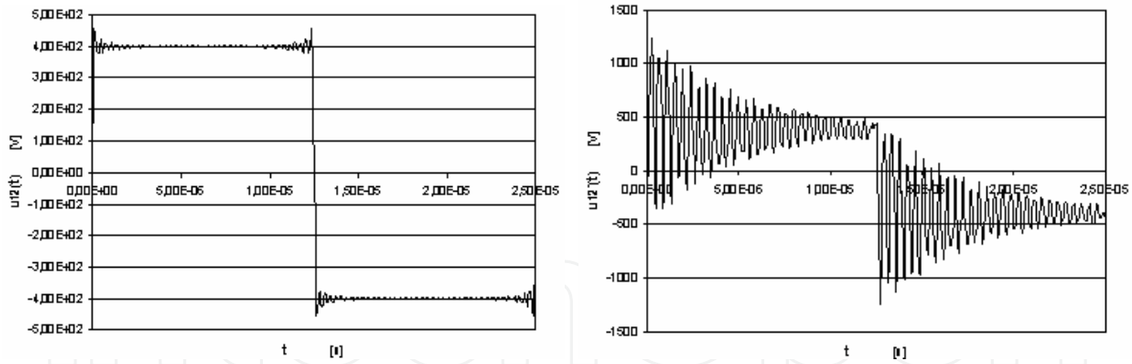

a) b)

Fig. 25. Synthesis of results a) input voltage u_{12}; b) output voltage $u_{12'}$

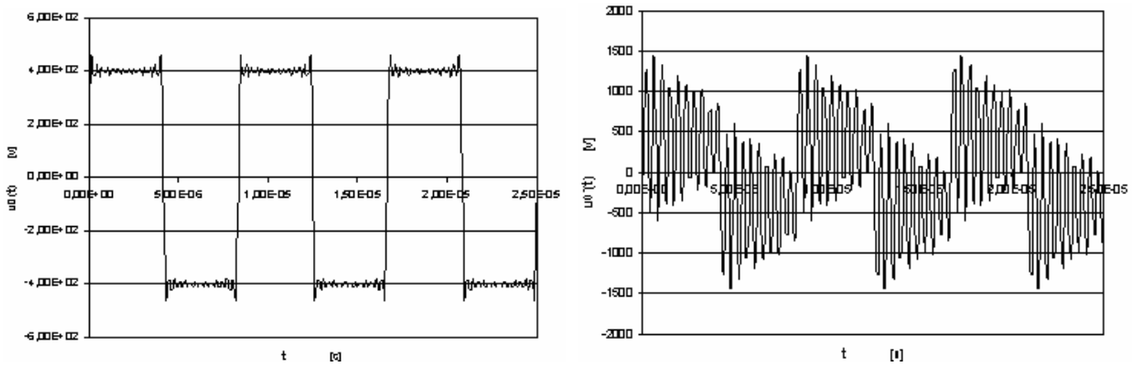

a) b)

Fig. 26. The potential of the a) source node; b) load node

The simulation results are displayed in the following Fig. 27 and measured in the Fig. 28. The coincidence between the courses obtained by analytical calculation, simulation method and by measurement is evident. So we can just suppose, that the derived relations are correct.

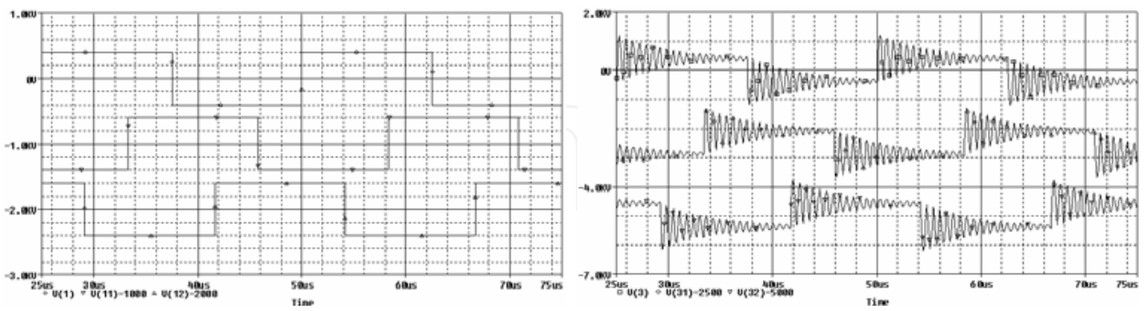

a) b)

Fig. 27. Simulation results of three phase non-harmonic a) input voltages; b) output voltages

6. Electromagnetic coupling

The electromagnetic coupling is typical for galvanically separated electrical circuits, between which the exchange of the electromagnetic energy exists in the form of the radiated and absorbed power.

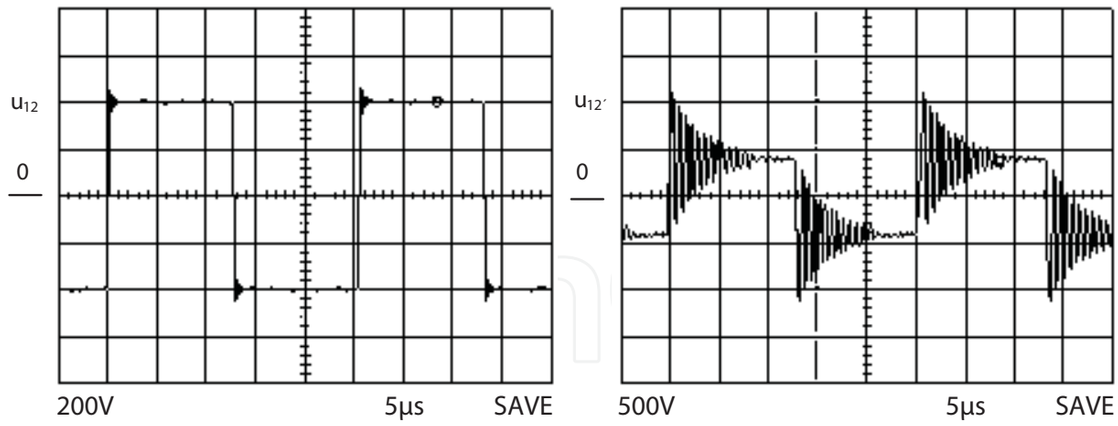

Fig. 28. Measured three phase non-harmonic a) input voltage u_{12}; b) output voltage $u_{12'}$

Let the mutual influence of two separated circuits be investigated. We come out from the first two Maxwell's equations in general form, defined by the vector potential. Let it is suppose, that the energy exchange is done through the air.

$$\overline{E} = -\nabla\varphi - \frac{\partial \overline{A}}{\partial t} \tag{49}$$

$$\overline{B} = \nabla \times \overline{A} \tag{50}$$

The potential φ and magnetic vector potential $\overline{A}$ investigation is leading to the solution of the partial-differential equations of the second order. The volume density of the environ charge is defined by ρ and the current density of conductor surface by $\overline{J}$.

$$\nabla^2\varphi - \frac{1}{c^2}\frac{\partial^2\varphi}{\partial t^2} = -\frac{\rho}{\varepsilon_0} \tag{51}$$

$$\nabla^2\varphi - \frac{1}{c^2}\frac{\partial^2\varphi}{\partial t^2} = -\frac{\rho}{\varepsilon_0} \tag{52}$$

Also next condition must to fulfilled by the searched solution (c is velocity of light):

$$\nabla.\overline{A} = -\frac{1}{c^2}\frac{\partial\varphi}{\partial t} \tag{53}$$

The relations for potential φ and magnetic vector potential $\overline{A}$ expressed for position 1 in dependence on the source parameters at the point 2 can be obtained by mathematical solving. For simplification of solution it will be supposed, that the length $\overline{l_i}$ of conductor element is so small in comparison with the vector length $\overline{r}_{12} = \overline{r}_i$, that the distances of the beginning and finishing points of conductor element of length, measured from the point 1, are the same. Situation is pictured in Fig. 29. The direction of current density vector $\overline{J}$ is coincident with the direction of unit conductor vector $\overline{l}^0$.

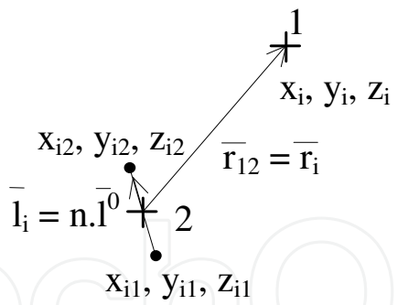

Fig. 29. Investigated point and element of the conductor length

$$\varphi(1,t) = \int \frac{\rho(2, t - \frac{r_{12}}{c})}{4\pi\varepsilon_0 r_{12}} dV_2 \tag{54}$$

$$\bar{A}(1,t) = \int \frac{\bar{J}(2, t - \frac{r_{12}}{c})}{4\pi\varepsilon_0 c^2 r_{12}} dV_2 \tag{55}$$

For the purpose of electrotechnical equipment EMC investigation let it is consider the expression for magnetic vector potential $\bar{A}$ will be related to the elementary radiator represented by the electrical dipole with the dipole moment $\bar{p}$. The variables $\bar{p}'$ and $\bar{p}''$ represent first and second derivation of the dipole moment vector according the time.

$$\bar{p}_i = q\bar{l}_i = \int i dt \bar{l}_i \quad \bar{p}_i' = \frac{dq}{dt}\bar{l}_i = i\bar{l}_i \quad \bar{p}_i'' = \frac{di}{dt}\bar{l}_i \tag{56}$$

The optional current course can be expressed by Fourier series as sum of the DC component and *k* components of individual harmonic functions:

$$i = C_0 + \sum_{k=1}^{n\to\infty} C_k \sin(k\omega t + \psi) = I_0 + \sum_{k=1}^{n\to\infty} I_{mk} \sin(k\omega t + \psi) \tag{57}$$

Dipole moment and its time derivations then have the forms:

$$\bar{p}_i = I_0 t l_i \bar{l}_i^0 - \sum_{k=1}^{n\to\infty} p_k \cos(k\omega t + \psi)\bar{l}_i^0 \quad \bar{p}_i' = I_0 l_i \bar{l}_i^0 + \sum_{k=1}^{n\to\infty} k\omega\, p_k \sin(k\omega t + \psi)\bar{l}_i^0 \quad \bar{p}_i'' = \sum_{k=1}^{n\to\infty} (k\omega)^2 p_k \cos(k\omega t + \psi)\bar{l}_i^0 \tag{58}$$

The next equation describes the magnetic vector potential $\bar{A}_i$ of electric dipole.

$$\bar{A}_i(1,t) = \frac{1}{4\pi\varepsilon_0 c^2} \frac{\bar{p}_i'(t - \frac{r_i}{c})}{r_i} \tag{59}$$

By its substitution into the equation (50) the resulting relation for magnetic intensity vector $\bar{H}_i$ of the electromagnetic field will be obtained. It can be expressed by the components of the 3D Cartesian system:

$$\bar{H}_i = \frac{\bar{B}_i}{\mu} = \frac{\nabla \times \bar{A}_i}{\mu} = \bar{H}_x + \bar{H}_y + \bar{H}_z = \frac{1}{4\pi} \frac{\left[\bar{p}_i^{\,\prime} + \left(\frac{r_i}{c} \right) \bar{p}_i^{\,\prime\prime} \right]_{t-\frac{r_i}{c}} \times \bar{r}_i}{r_i^3} \tag{60}$$

Electric intensity $\bar{E}_i$ vector calculation, as the second component of electromagnetic field, will be deduced from condition (53). The found solution of the partial-differential equation of the second order for magnetic vector potential $\bar{A}$ must fulfill this condition.

$$\nabla . \bar{A}_i = -\frac{1}{4\pi\varepsilon_0 c^2} \frac{\left(\bar{p}_i^{\,\prime}(t - \frac{r_i}{c}) + \left(\frac{r_i}{c} \right) \bar{p}_i^{\,\prime\prime}(t - \frac{r_i}{c}) \right) \bar{r}_i}{r_i^3} = -\frac{1}{c^2} \frac{\partial \varphi_i}{\partial t} \tag{61}$$

The time gradient of potential at the investigated place is necessary to express from the above-mentioned equation.

$$\frac{\partial \varphi_i}{\partial t} = \frac{1}{4\pi\varepsilon_0} \frac{\left(\bar{p}_i^{\,\prime}(t - \frac{r_i}{c}) + \left(\frac{r_i}{c} \right) \bar{p}_i^{\,\prime\prime}(t - \frac{r_i}{c}) \right) \bar{r}_i}{r_i^3} \tag{62}$$

The relation for potential will be received after the integration.

$$\varphi_i = \frac{1}{4\pi\varepsilon_0} \frac{\left(\bar{p}_i(t - \frac{r_i}{c}) + \left(\frac{r_i}{c} \right) \bar{p}_i^{\,\prime}(t - \frac{r_i}{c}) \right) \bar{r}_i}{r_i^3} + K \tag{63}$$

Integral constant K expresses a possible existence of the electrostatic field. It should be omitted during the investigation of electromagnetic wave spreading and so the final formula can be simplified.

By substitution of the obtained dependencies for potential φ and magnetic vector potential $\bar{A}$ into the equation (49) and by its modification the searched formula for electric field intensity $\bar{E}$ vector caused by harmonic pulsating dipole can be expressed.

$$\bar{E} = \bar{E}_x + \bar{E}_y + \bar{E}_z = -\frac{1}{4\pi\varepsilon_0 r_i^3} \left[-\bar{p}_i(t - \frac{r_i}{c}) - \left(\frac{r_i}{c} \right) \bar{p}_i^{\,\prime}(t - \frac{r_i}{c}) - 3 \frac{\left(\left(\bar{p}_i(t - \frac{r_i}{c}) + \left(\frac{r_i}{c} \right) \bar{p}_i^{\,\prime}(t - \frac{r_i}{c}) \right) \bar{r}_i \right) \bar{r}_i}{r_i^2} + \frac{\bar{p}_i^{\,\prime\prime}(t - \frac{r_i}{c})}{c^2} \left(r_i^2 - \bar{r}_i \bar{r}_i \right) \right] \tag{64}$$

Note, that above-mentioned condition $l = \sum_{i=1}^{m \to \infty} l_i$ for total length of the investigated current conductor is valid, too.

Let's investigate the EMC from the viewpoint of electromagnetic coupling. For this purpose it is satisfactory to analyze the value of resulting vectors $\bar{E}$ and $\bar{H}$, at the given position, which is created by the superposition of individual vectors $\bar{E}_i$ and $\bar{H}_i$ of power radiated from all devices and their parts situated inside the investigated environs. If the non-harmonic currents supply the circuits of radiated sources, then the superposition method of

individual harmonic components of Fourier series needs to be applied for the resulting vectors $\bar{E}$ and $\bar{H}$ searching. It is also necessary to keep in mind that the additional induced voltage is developed inside the individual loops of investigated circuit due to electromagnetic coupling existence. These voltages can affect circuit basic functionality. The equipment EMC investigation thus means the voltage value stating in such a way that the question of circuit functionality can be answered and circuit immunity stated.

$$u_i = u_{imag} + u_{ielec} = -\frac{d\psi}{dt} + \int \bar{E} d\bar{l} = -\frac{d\bar{B}\bar{S}}{dt} + \int \bar{E} d\bar{l} = -\mu_0 S \sum_{i=1}^{m\to\infty} \frac{\Delta H_i}{\Delta t} \cos\alpha_i + \sum_{i=1}^{m\to\infty} E_i l_i \cos\beta_i \qquad (65)$$

Let the correctness verification of derived equations be done by induced voltage oscillograph measurement inside the circuit connected according to Fig. 30. As the source of

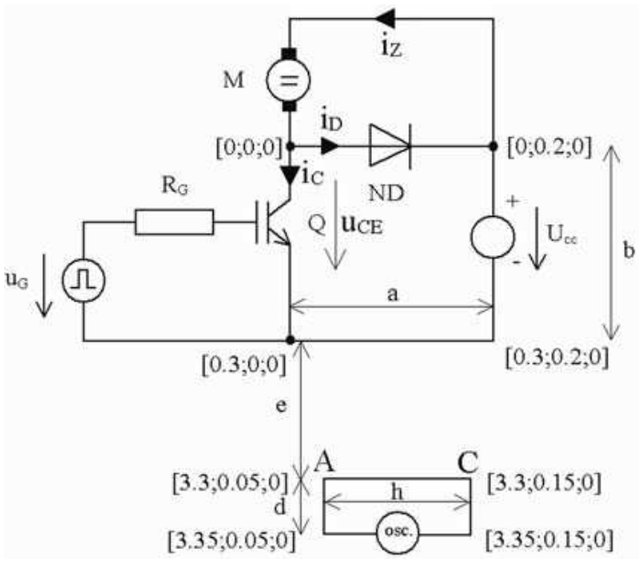

Fig. 30. Investigated circuit scheme.

radiation the one quadrant impulse converter is used with the same working parameters as presented in the previous subchapters. Let the circuit location be on the x, y plane. The co-ordinates of Cartesian coordinate system describe individual key points of connection. On the basis of the results obtained from Fourier and transient analyses offered by PSPICE program the DC and the first nine components of Fourier series can express the courses of all power circuit currents and transistor voltage. The final simulation and measured results are presented in figure Fig. 31.

On the basis of the obtained coefficients let the Excel program do the verification synthesis of transistor current course. The result is introduced in Fig. 32. By comparing courses one can state that due to considering only first nine members of Fourier series the peak transistor current generated by the commutation charge of diode was neglected and also the certain undulation was infiltrated. But otherwise its shape is identical with the real measured current course.

By substituting the individual harmonic amplitudes and phases to the Fourier series one can obtain the analytical form of investigated non-harmonic currents. By their application in the equations (60) and (64) it is possible to receive the searched solution for the electromagnetic

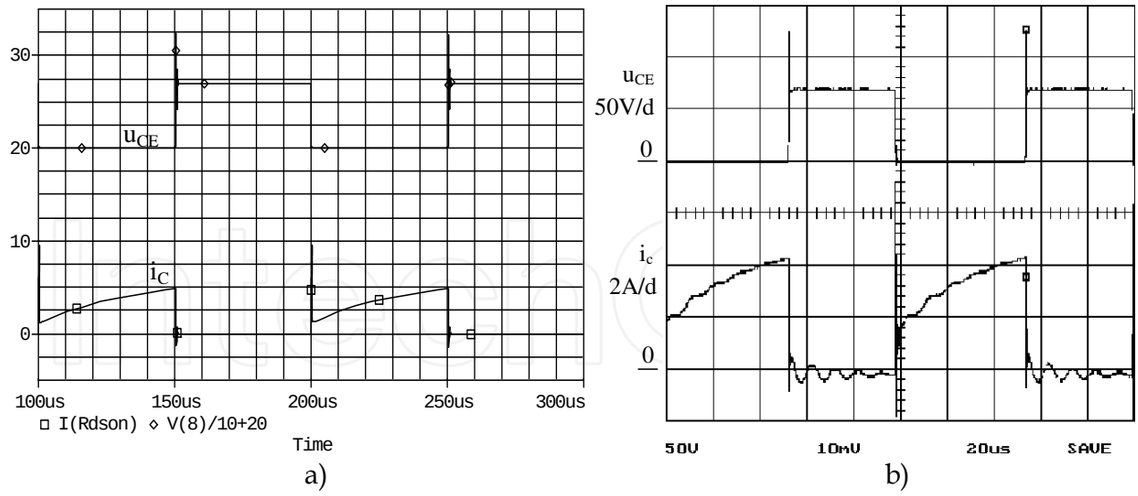

Fig. 31. Transistor voltage and current obtained by a) simulation; b) measurement

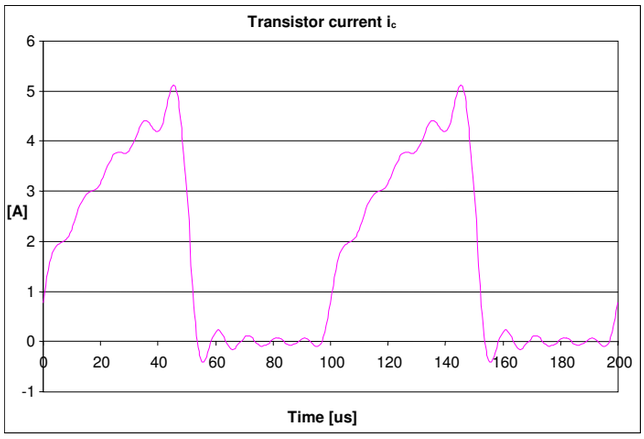

Fig. 32. Transistor current - synthesis by 9 members of Fourier series

wave components. The induced voltage generated by the magnetic component of electromagnetic wave can be stated in such a way that the values of axis components of magnetic intensity vector will be calculated at the position in the centre of impacted loop. If the loop dimensions are omissible towards the length of electromagnetic wave, then the magnetic field intensity inside the loop can be allowed to be constant at the given moment and the induced voltage can be calculated according to the equation:

$$u_{imag} = -\mu_0 S \left[\frac{\sqrt{H_x^2(t+\Delta t) + H_y^2(t+\Delta t) + H_z^2(t+\Delta t)}}{\Delta t} - \frac{\sqrt{H_x^2(t) + H_y^2(t) + H_z^2(t)}}{\Delta t} \right] \tag{66}$$

where S is the surface of impacted loop which represents the impacted electrical circuit.
The induced voltage generated by the electric component of electromagnetic wave can be stated in such a way that the values of axis components of electric intensity vector at the positions A[3.3;0.05;0] and C[3.3;0.15;0] will be found. The induced voltage value then should be calculated on the basis of the well-known relation from the field of theoretical

electrical engineering; however, only if we take into consideration the fact that the moving electromagnetic wave changes its own intensity by the value ΔE_x (or ΔE_y) during its transition time $\Delta t' = d/c$ (or $\Delta t'' = h/c$) along the investigated loop.

$$u_{ielec} = \left(E_{xA}(t+\Delta t') - E_{xA}(t)\right)d + \left(E_{xC}(t+\Delta t') - E_{xC}(t)\right)d + \left(E_{yA}(t+\Delta t'') - E_{yA}(t)\right)h + \left(E_{yC}(t+\Delta t'') - E_{yC}(t)\right)h \quad (67)$$

Resulting induced voltage, calculated as the superposition of its magnetic and electric compounds, does not provide satisfactory graphical representation in analytical form. The numerical method of searching time depending solution and the graphical presentation are more advantageous in this case because the computer programs currently available, for example, the Excel program, allow its application very easily. On the basis of the previous equation calculations, which were done for two periods of basic harmonics, one can obtain the graphical interpretation of resulting induced voltage inside the impacted loop, which is shown in the Fig. 33.

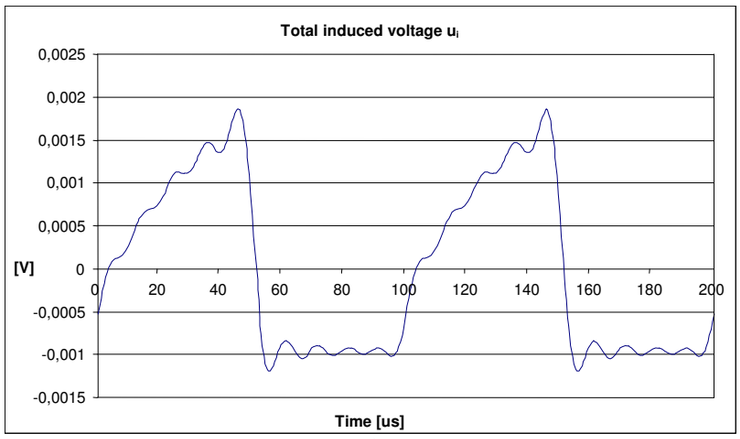

a)

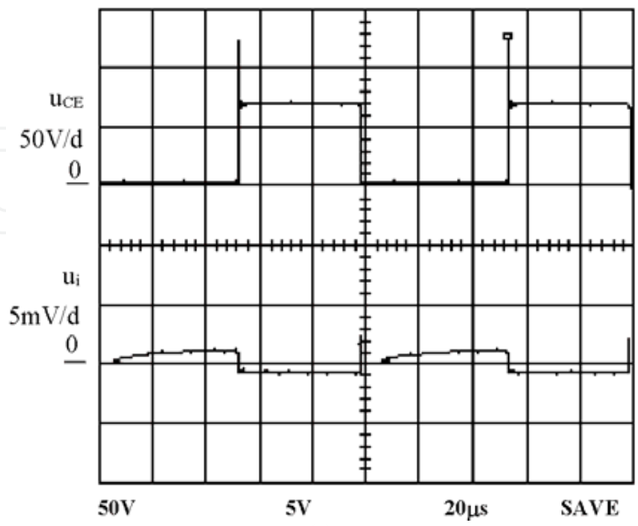

b)

Fig. 33. Total induced voltage u_i inside the investigated loop a) calculated; b) measured

By comparing the simulated and measured results one can find out that positive amplitudes reach approximately the same values 1.8 mV and similarly the negative amplitudes have the values 1 mV. The existing ripple and the absence of short positive voltage impulse with the amplitude 2.5 mV inside the induced voltage course obtained by simulation is caused by considering only the first nine components of Fourier series. Generally it is possible to say that there exists a relatively great coincidence between the simulated and measured results. Thus the correctness of derived equations is confirmed as well as the fact that if higher number of Fourier series components are used the better coincidence of both type results will be obtained. It means that during the electromagnetic coupling investigation, as one part of general EMC investigation, it is necessary to reconsider the compromise between the number of Fourier series components and the required calculation precision.
The above-mentioned simulated and measured results are sufficiently identical with the theoretical results and so they confirm the correctness of derived equations. Such a way they can be used for predictive stating of EMC quality of individual new electrotechnical products (Williams, 2001).
Based on the performed analysis also we can find out that the intensity of electromagnetic coupling is directly proportional to the amount and the time change slope of circuit current, which is radiating the electromagnetic energy. In the same way electromagnetic coupling intensity depends on the length of this circuit. It is also directly proportional to the surface and the length values of disturbed circuit. It is indirectly proportional to the distance between the interference source and the disturbed circuits, to the reflection coefficient and to the permeability and permittivity values of space between the both circuits.

7. Conclusion

The performed analysis enables constructers to improve the EMC parameters of the newly constructed devices not only by expensive testing measurements, but also in advance, by the theoretical analysis and simulation. They can state its supposed and required properties by a predictive method based upon the results introduced in this chapter (Kováčová et al., 2006). The improving of EMC will thus be more comfortable, cheaper, easier and quicker.
All results presented in this chapter has been prepared under the support of Slovak grant projects VEGA No.1/0660/08, KEGA No. 003-003TUKE-4/2010, KEGA No. 3/6386/08, KEGA No. 3/6388/08.

8. References

Clayton, R. P. (1992). *Introduction to electromagnetic compatibility,* John Wiley & Sons, ISBN 0-471-54927-4 , New York, USA

Kováčová, I. ; Kováč, D. & Kaňuch, J. (2006). *EMC from the look of the theory and practice,* BEN Publisher, ISBN 80-7300-202-7, Prague, 2006, Czech Republic

Kůs, V. (2002). *The influence of semiconductor converters on feeding net,* BEN Publisher, ISBN 80-7300-062-8, Prague, Czech Republic

Montrose, M. & Nakauchi, E. (2004). *Testing for EMC Compliance: Approaches and Techniques,* John Wiley & Sons, ISBN 0-471-43308-X, New York, USA

Tihanyi, L. (1995). *Electromagnetic compatibility in power electronics,* IEEE Press, ISBN 0-7803-0416-0, Piscataway,USA

Vaculíková, P. & Vaculík, E. (1998). *Electromagnetic compatibility of electrical engineering systems,* Grada Publisher, ISBN 80-7169-568-8, Prague, Czech Republic

Williams, T. (2001). *EMC for Product Designers,* An imprint of Elsevier Science, ISBN 0-7506-4930-5, Oxford, UK

New Trends in Technologies: Control, Management, Computational Intelligence and Network Systems
Edited by Meng Joo Er

ISBN 978-953-307-213-5
Hard cover, 438 pages
Publisher Sciyo
Published online 02, November, 2010
Published in print edition November, 2010

The grandest accomplishments of engineering took place in the twentieth century. The widespread development and distribution of electricity and clean water, automobiles and airplanes, radio and television, spacecraft and lasers, antibiotics and medical imaging, computers and the Internet are just some of the highlights from a century in which engineering revolutionized and improved virtually every aspect of human life. In this book, the authors provide a glimpse of the new trends of technologies pertaining to control, management, computational intelligence and network systems.

How to reference
In order to correctly reference this scholarly work, feel free to copy and paste the following:

Dobroslav Kovac and Irena Kováčová (2010). EMC Aspect as Important Parameter of New Technologies, New Trends in Technologies: Control, Management, Computational Intelligence and Network Systems, Meng Joo Er (Ed.), ISBN: 978-953-307-213-5, InTech, Available from: http://www.intechopen.com/books/new-trends-in-technologies--control--management--computational-intelligence-and-network-systems/emc-aspect-as-important-parameter-of-new-technologies

INTECH
open science | open minds

InTech Europe
University Campus STeP Ri
Slavka Krautzeka 83/A
51000 Rijeka, Croatia
Phone: +385 (51) 770 447
Fax: +385 (51) 686 166
www.intechopen.com

InTech China
Unit 405, Office Block, Hotel Equatorial Shanghai
No.65, Yan An Road (West), Shanghai, 200040, China
中国上海市延安西路65号上海国际贵都大饭店办公楼405单元
Phone: +86-21-62489820
Fax: +86-21-62489821

IntechOpen